Spring 5-22-2020

Application of Monte Carlo (MC) method and Unscented Transformation (UT) method into Trajectory Prediction of a Dropped Cylinder in Two Dimensions

Yi Li
University of New Orleans, yli25@uno.edu

Application of Monte Carlo (MC) method and Unscented Transformation (UT) method into Trajectory Prediction of a Dropped Cylinder in Two Dimensions

A Thesis

Submitted to the Graduate Faculty of the
University of New Orleans
in partial fulfillment of the
requirements for the degree of

Master of Science
in
Engineering
Naval Architect and Marine

by

Yi Li

B.S. Qingdao Technological University, 2015

May, 2020

Acknowledgement

I would like to express my sincerest appreciation to a number of people without whom this dissertation would not have been possible.

To my advisor, Dr. Vincent Xiaochuan Yu, who is always a source of knowledge and inspiration for me.

To my professors, Dr. Lothar Birk, Dr. Brandon Taravella and Dr. Nikolas Xiros, who also provide me invaluable and insightful thinking and guidance during my research.

To all my friends and colleagues, without whom, my life during the master study in UNO would become much harder.

To my beloved parents, who continuously support and encourage me throughout my study and research.

Table of contents

List of Figures

List of Tables

Nomenclature

OXZ	Global coordinate system
oxz	Local coordinate system fixed on the cylinder
X	X-axis points to the right along the still water surface
Z	Z-axis perpendicular to the still water surface and point upward
U_1	Velocity component for surge
U_3	Velocity component for heave
Ω_2	Velocity component for pitch
β	The instantaneous rotational angle between the *x*-axis and the *X*- axis
m	Mass of the cylinder
M_{55}	Moment of inertia along the pitch direction
m_{33}	Added mass along heave direction from the strip theory
m_{55}	Added mass along pitch direction from the strip theory
m_t	2D added mass along heave direction at the trailing edge
x_t	Longitudinal position of effective trailing edge
g	Acceleration of the gravity
ρ	Density of the water
r	Volume of the cylinder
D	Diameter of the cylinder
v	Kinematic viscosity of the water
L	Length of the cylinder
C_{dx}	Drag coefficient along the x-direction
C_{dz}	Drag coefficient along the z-direction
F_{dx}	Drag force along the direction of surge
F_{dz}	Force component along the direction of heave

M_{dy}	Force component along the direction of pitch
x_k	State at time index k
k	Time index
$\dot{x}_k = f_k(x_k)$	The state space model
x_{k+1}=$f_k^d(x_k)$	The discretized state space model
$x(\bar{x}, P_x)$	Random variable x with mean $\bar{x}$ and covariance P_x
ς	The set of sigma point
n_x	Dimension of random variable x
$\sqrt{\cdot}$	Cholesky decomposition
$(\sqrt{\cdot})_i$	The i-th column of the decomposed matrix
w	Tuning weight
$\mathcal{N}(\bar{x}, \sigma)$	Gaussian distribution with mean $\bar{x}$ and standard deviation
$x \sim \mathcal{N}(\bar{x}, \sigma)$	State x_k under the Gaussian distribution $\mathcal{N}(\bar{x}, \sigma)$
A_{olp}	Overlap area between the predicted drop range, and the one from the experimental envelope
A_{ee}	The area covered by experimental envelope
L_{olp}	Overlap length
L_{ee}	Experimental envelope length at the bottom
R_A	$\frac{A_{olp}}{A_{ee}}$
R_L	$\frac{L_{olp}}{L_{ee}}$

Abbreviation

MC	Monte Carlo
UT	Unscented Transformation
ABS	American Bureau of Shipping
DNV	Det Norske Veritas
BP	British Petroleum Company
2-D	Two-dimension
3-D	Three-dimension

Abstract

Monte Carlo (MC) method is one of the most prevailing methods to solve stochastic problems. However, as a method of using random samples to calculate statistics, its accuracy heavily depends on the size of sample. A systematic formulation the cylinder's three-degree-of-freedom (surge, heave and pitch) of motions is presented as a state space model. It is assumed that the small disturbances at its initial state i.e., the velocity and the drop angle of each degree, follow a Gaussian distribution. This non-linear prediction problem can be solved by using the MC method and unscented transformation (UT). By comparing the statistical results of these two methods, we conclude that for the problem of dropping a cylinder into water freely, the UT method will be comparatively better when considering both accuracy and calculation requirements.

Keywords: Trajectory prediction, Drop cylinders, State space model, Offshore operations, Monte Carlo method, Unscented transformation method

I. Introduction

Dropped objects increase the risk of offshore installations and are one of the leading causes of accidents in the oil and gas industry (DORIS, 2016). The ABS Guide (2010) proposes an overall assessment procedure for assessing damage caused by falling objects, which may have been caused by failure of the supply vessel's lifting operations or storms. The ABS guidelines also highlight their lack specialized technology to predict the trajectory of dropped objects and the consequences of subsequent impacts on other structures and equipment. Therefore, predicting the trajectory of an object falling into the water and its falling point is very important to protect the oil and gas production equipment on the seabed.

Aanesland (1987) numerically and experimentally studied falling water pipes. He observed six different fall patterns of the drill pipe model during model tests. DNV (2010) endorsed these findings and included them in the specification. It was found from the model tests that the most important factors are the angle of attack after water entry and the falling height, etc. A slight difference in the initial drop angle will result in a different drop point. In numerical simulation, two-dimensional (2D) maneuvering equations were applied to describe the motion of the drill pipe, which were further corrected by considering the trailing edge effect and the viscous effect of a slender object (Newman, 1977). It should also be known that using 2D equations to describe 3D motion may cause some errors, so the axial rotation of the cylinder should also be considered. In general, the results of numerical analysis can be verified by model testing. Luo and Davis (1992) also simulated the 2D motion of falling objects by solving differential equations of motion. Their descriptive parameter studies were performed in a computer program called DELTA. The program found that the falling point of the cylinder in the horizontal direction of the sea floor was greatly affected by the drop angle. In addition, the maximum horizontal speed of an object depends on its drop height and drop angle, and the tangential drag coefficient seems to have little effect on the trajectory. At the same time, Colwill and Ahilan used the same computer program, DELTA, to perform multiple numerical studies on the trajectories of two falling drill casings. These studies confirmed that the drop height and initial drop angle above the waterline surface are key parameters that affect horizontal velocity. The reliability-based impact analysis successfully established the relationship between the impact speed and its probability of overtaking (Colwill and Ahilan, 1992). Katteland and Øygarden (1995) assessed the risks associated with falling objects in the offshore oil and gas industry. They established four distributions to describe the spreading of dropped objects from an offshore installation at deep water In their proposed paradigm, the effects of wind, waves and currents are also considered.

After the BP oil spill crisis in 2010, research related to submarine pipeline safety and risk assessment became hot. Awotahegn (2014) conducted a series of model tests to investigate the trajectory and seafloor distribution of two drill pipes (8 and 12 inches) falling into calm waters from a defined height above the water surface. He mapped and statistically analyzed the distribution of landing points on the sea floor from 0 ° to 90 °. After comparing them with the results of the simplified method (DNV, 2010), he considered that the simplified method of DNV is relatively conservative. In addition, the latest numerical analysis of falling cylinders includes Xiang et al. (2016), Xiang et al. (2017a), Xiang et al. (2017b), and Xiang et al. (2019).

In this thesis, Aanesland's (1987) three-degree-of-freedom (3DOF) motion (Surge, heave and pitch) equations are used to describe the two-dimensional motion of a cylinder. By constructing a state space model for this system of equations, we can easily derive the change in resistance of a cylinder in water over time, and study the effects of various factors, such as the angle of water entry and rolling frequency, on the cylinder trajectory and landing point. Previous numerical studies and experimental tests have shown that the falling trajectory of a cylinder depends to a large extent on these factors (Xiang et al., 2016), (Xiang et al., 2017a) and (Xiang et al., 2017b). Since the distribution of the landing points of the falling cylinders appears to be random, when predicting its trajectory, random disturbances will be experimentally added in the initial state. On the one hand, the MC method, as the most common random sampling method, is used in the statistical analysis of calculating the corresponding trajectory of a cylinder under different falling angle conditions. On the other hand, the UT method, as a well-known trajectory tracking algorithm in electronic engineering, has been adopted because it has better results than other similar methods in dealing with this problem. The trajectory envelopes calculated by the two methods are compared with the 2D experimental envelopes published in (DNV, 2010). Two performance parameters are proposed to evaluate the accuracy of the two methods for predicting trajectories.

II. Theories

2.1 Equations of motion (EOM) for dropped cylinders in two dimensions (2D)

Two-dimensional (2D) theory involves two coordinate systems, as shown in Figure 1. OXZ represents the global coordinate system, where the X-axis points to the right along the still water surface, and the Z axis is perpendicular to the still water surface and points upward. On the other hand, the local coordinate system, oxz, is fixed on the cylinder. The axis of the cylinder is the x-axis, and the origin o of the coordinate system oxz is located at the center of gravity of the cylinder. If the cylinder is placed horizontally on the water at the beginning, the two coordinate systems coincide. Because this article assumes that the cylinder is rigid and slender and its mass is evenly distributed, its center of mass and geometric center coincides. Aanesland (1987) simplified the problem into a two-dimensional one, which consider motions in the x-z plane only. The velocity components are U_1 (surge), U_3 (heave) and Ω_2 (pitch). The equations of motion are as follows:

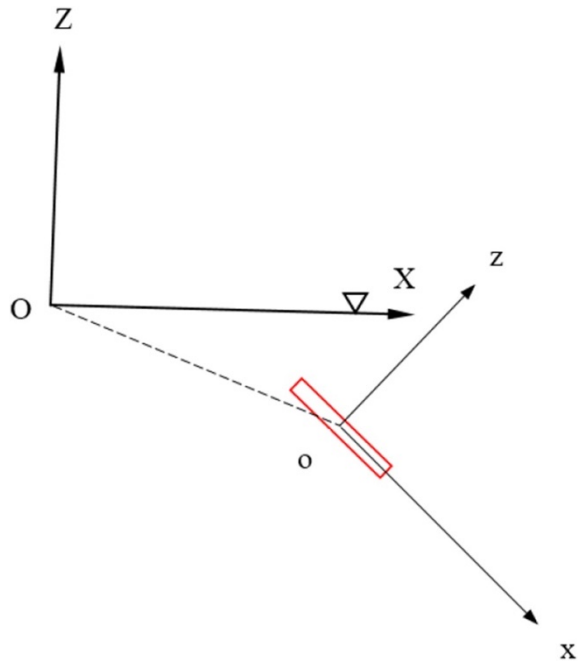

Figure 1 The 2D coordinate system

$$(m-\rho\nabla)gsin(\beta)+F_{dx}=m\dot{U}_1 \tag{1}$$

$$-(m-\rho\nabla)cos(\beta)+F_{dz}=\{U_1m_1U_3-U_1(x_tm_t)\Omega_2+m_{33}\dot{U}_3\}+m(\dot{U}_3-U_1\Omega_2) \tag{2}$$

$$M_{dy}=\{-U_1(m_{33}+x_tm_t)U_3+U_1{x_t}^2m_t\Omega_2+m_{55}\dot{\Omega}_2\}+M_{55}\dot{\Omega}_2 \tag{3}$$

where

β: The instantaneous rotational angle between the *x*-axis and the *X*- axis.

m: Mass of the cylinder.
M_{55}: The moment of inertia in the pitch direction.

m_{33}: Added mass in heave direction from the strip theory.

m_{55}: Added mass in pitch direction from the strip theory.

m_t: 2D added mass in heave direction at the trailing edge.

x_t: Longitudinal position of effective trailing edge.

g: Acceleration of the gravity. ρ: the density of the water.
r: Volume of the cylinder.

It should be noted that the equations (1) – (3) state the motion in the body-fixed coordinate system oxz. Since the ends of the cylinder are not sharp, the longitudinal position with an effective trailing edge x_t is introduced. Since the abrupt ends of the cylinder do not satisfy the smooth change in geometry assumed in the slender body theory. An additional force component is included to consider this trailing edge effect for a long slender body as shown in curly brackets on the right side of (2)–(3) (Newman, 1977). The remaining terms are inertial forces and moments.

The viscous forces and moment, F_{dx}, F_{dz}, M_{dy} are represented as

$$F_{dx} = -0.664\pi\sqrt{\upsilon\rho^2 L}U_1\sqrt{|U_1|} - \frac{1}{8}\rho\pi C_{dz}D^2U_1|U_1| \tag{4}$$

$$F_{dz} = 0.5\int_{-0.5L}^{0.5L}\rho C_{dz}DU_z(x)|U_z(x)|dx \tag{5}$$

$$M_{dy} = -0.5\int_{-0.5L}^{0.5L}\rho C_{dz}DxU_z(x)|U_z(x)|dx \tag{6}$$

The frictional drag represented by the first term in (4) is obtained from the turbulent boundary layer theory (Schlichting, 1979), and the second term represents the form drag (Hoerner, 1965). Apply Morrison's equation in (5) and (6) to obtain the force component of the cylinder in the direction of the heap and pitch. The unknown parameter $U_z(x)$ is the local relative speed between the cylinder and the water in the z-axis direction. It can be expressed as

$$U_z(x) = -(U_3 - \Omega_2 x), -0.5L < x < 0.5L \tag{7}$$

Substitute (7) into (5)– (6), we obtain

$$F_{dz} = -0.5\rho C_{dz}D\int_{-0.5L}^{0.5L}(U_3 - \Omega_2 x)|U_3 - \Omega_2 x|dx \tag{8}$$

$$M_{dy} = 0.5\rho C_{dz}D\int_{-0.5L}^{0.5L}x(U_3 - \Omega_2 x)|U_3 - \Omega_2 x|dx \tag{9}$$

where

D: Diameter of the cylinder
v: Kinematic viscosity of the water
L: Length of the cylinder

C_{dx}: Drag coefficient along the x-direction

C_{dz}: Drag coefficient along the z-direction

In numerical simulation, the following relations are used to transform motion in the local coordinate system into motion in the global system:

$$\begin{pmatrix}\dot{X}\\ \dot{Y}\end{pmatrix}=\begin{bmatrix}cos\beta & -sin\beta\\ sin\beta & cos\beta\end{bmatrix}\begin{pmatrix}U_1\\ U_3\end{pmatrix} \tag{10}$$

where the initial value $[\mathrm{X}_0,\mathrm{Y}_0]=[0,0]$, $\dot{\beta}$=Ω_2.

2.2 The state space model

The state-based nonlinear dynamic system can formulate the equations of the motion of the dropped cylinder in two-dimensions above. The model of this system can be written as

$$\dot{x}_k=f_k(x_k)=\begin{bmatrix}\frac{1}{m}(m-\rho\nabla)g\sin x_{4,k}-\frac{0.664}{m}\pi\sqrt{v\rho^2L}x_{1,k}\sqrt{|x_{1,k}|}-\frac{1}{8m}\rho\pi C_{dx}D^2x_{1,k}|x_{1,k}|\\ \frac{1}{m_{33}+m}\left[-(m-\rho\nabla)g\cos x_{4,k}+F_{dz}-m_tx_{1,k}x_{2,k}+x_tm_tx_{1,k}x_{3,k}+mx_{1,k}x_{3,k}\right]\\ \frac{1}{m_{55}+M_{55}}\left[M_{dy}+(m_{33}+x_tm_t)x_{1,k}x_{2,k}-{x_t}^2m_tx_{1,k}x_{3,k}\right]\\ \dot{x}_{3,k}\end{bmatrix} \tag{11}$$

where $x_k=\left[x_{1,k},x_{2,k},x_{3,k},x_{4,k}\right]'=\left[U_{1,k},U_{3,k},\Omega_{2,k},\beta_k\right]'$.

$$F_{dz,k}=\begin{cases}\frac{1}{24}\rho C_{dz}DL^3{x_{3,k}}^2+\frac{1}{2}\rho C_{dz}DL{x_{2,k}}^2 & x_{3,k}<0,\frac{x_{2,k}}{x_{3,k}}\geq\frac{L}{2}\\ -\frac{1}{2}\rho C_{dz}D\left(\frac{1}{12}{\mathrm{L}_{3,k}}^2+L{x_{2,k}}^2\right) & x_{3,k}<0,\frac{x_{2,k}}{x_{3,k}}\leq\frac{L}{2}\\ \frac{1}{2}\rho C_{dz}D\left(\frac{1}{12}\frac{{x_{2,k}}^2}{x_{3,k}}+\frac{1}{2}L^2x_{2,k}x_{3,k}\right) & x_{3,k}<0,\frac{x_{2,k}}{x_{3,k}}\in\left(-\frac{L}{2},\frac{L}{2}\right)\\ -\frac{1}{2}\rho C_{dz}D\left(\frac{1}{12}{\mathrm{L}_{3,k}}^2+L{x_{2,k}}^2\right) & x_{3,k}>0,\frac{x_{2,k}}{x_{3,k}}\geq\frac{L}{2}\\ \frac{1}{24}\rho C_{dz}DL^3{x_{3,k}}^2+\frac{1}{2}\rho C_{dz}DL{x_{2,k}}^2 & x_{3,k}>0,\frac{x_{2,k}}{x_{3,k}}\leq\frac{L}{2}\\ -\frac{1}{2}\rho C_{dz}D\left(\frac{2}{3}\frac{{x_{2,k}}^2}{x_{3,k}}+\frac{1}{2}L^2x_{2,k}x_{3,k}\right) & x_{3,k}<0,\frac{x_{2,k}}{x_{3,k}}\in\left(-\frac{L}{2},\frac{L}{2}\right)\\ -\frac{1}{2}\rho C_{dz}DL|x_{2,k}|x_{2,k} & x_{3,k}=0\end{cases}$$

And

$$M_{dy,k}=\begin{cases}\frac{1}{12}\rho C_{dz}DL^3x_{2,k}x_{3,k} & x_{3,k}<0,\frac{x_{2,k}}{x_{3,k}}\geq\frac{L}{2}\\ -\frac{1}{12}\rho C_{dz}DL^3x_{2,k}x_{3,k} & x_{3,k}<0,\frac{x_{2,k}}{x_{3,k}}\leq\frac{L}{2}\\ \frac{1}{2}\rho C_{dz}D\left(\frac{1}{32}L^4{x_{3,k}}^2+\frac{1}{4}L^2{x_{2,k}}^2-\frac{2}{3}\frac{{x_{3,k}}^4}{{x_{2,k}}^2}\right) & x_{3,k}<0,\frac{x_{2,k}}{x_{3,k}}\in\left(-\frac{L}{2},\frac{L}{2}\right)\\ -\frac{1}{12}\rho C_{dz}DL^3x_{2,k}x_{3,k} & x_{3,k}>0,\frac{x_{2,k}}{x_{3,k}}\geq\frac{L}{2}\\ \frac{1}{12}\rho C_{dz}DL^3x_{2,k}x_{3,k} & x_{3,k}>0,\frac{x_{2,k}}{x_{3,k}}\leq\frac{L}{2}\\ -\frac{1}{2}\rho C_{dz}D\left(\frac{1}{32}L^4{x_{3,k}}^2+\frac{1}{4}L^2{x_{2,k}}^2-\frac{2}{3}\frac{{x_{3,k}}^4}{{x_{2,k}}^2}\right) & x_{3,k}>0,\frac{x_{2,k}}{x_{3,k}}\in\left(-\frac{L}{2},\frac{L}{2}\right)\\ 0 & x_{3,k}=0\end{cases}$$

In the above model, a vector describing the unit state. x_k represents the unit state, including $U_{1,k}$, $U_{3,k}$, $\Omega_{2,k}$ and β_k. They represent the velocity in x direction, the velocity in z direction, pitch moment and angle, respectively, and k represents the k-th differential time.

2.3 Monte Carlo method

MC method is reliable under the premise of a large number of samples. According to the actual data detected in the drop experiment, this thesis demonstrates that there is a fluctuation at the initial state of the falling object, and the fluctuation is modeled to be the Gaussian distribution. Therefore, we add random perturbations that follow Gaussian distribution to the surge, sway, pitch, and the initial angle in the initial state. Their variances are

$$P_0=\left[10^{-4}\ m^2/s^2, 10^{-4}\ m^2/s^2, \left(\frac{\pi}{90}\right)^2\ rad^2/s^2, \left(\frac{\pi}{90}\right)^2\ rad^2\right].$$

Subsequently, since the initial state of the problem is described by four terms, when MC method is performed, the number of simulations is set to be a power of 4, such as 2^4, 3^4… After the simulation is completed, the x, z coordinates of each trajectory of falling cylinders on the x-axis and the z-axis are collected, then find the mean $\bar{x}$, $\bar{z}$ and variance σ_x, σ_z of all the trajectories, and obtain the envelope according to the confidence interval $[\bar{x}-\sigma_x,\ \bar{x}+\sigma_x]$ and $[\bar{z}-\sigma_z,\ \bar{z}+\sigma_z]$. Finally, we compare it with the actual experimental data. For a Gaussian distribution, when sigma range (the multiplier of σ) is 1, the probability of this event occurring is 0.6826.

2.4 Unscented transformation

In fact, the state space model described in Sec. 2.2 can be summarized as

$$\dot{x}_k = f_k(x_k) \tag{12}$$

or as a discretized model (e.g., using the Euler method with short time dt), which is the basic framework for nonlinear state prediction problem (Mendel and Oppenheim, 1995),

$$x_{k+1} = f_k^d(x_k) = x_k + dt \cdot f_k(x_k) \tag{13}$$

Due to the disturbance at the initial state x_0, the state $\{x_k\}$ can be regarded as a random process. The point prediction of nonlinear state x_k is used to predict the information about $x_{k+\lambda}$ at time k at some $\lambda > 0$. To obtain this information, a state space model (13) and measurements from the beginning to time k can be used (Anderson and Moore, 1979). From a statistical point of view, this information refers to the probability density function (pdf) of the state x_k at each time k or at least statistical information of interest (e.g., the mean and covariance).

The unscented transform (UT) method is a mathematical tool first proposed by Julier and Uhlman to solve the problem of nonlinear point prediction (Julier and Uhlmann, 1997) It is widely used for state estimation and parameter estimation (der Merwe and Wan, 2001) and (Wan and Merwe 2000). The UT method solves the problem by using a deterministic sampling method. It encodes statistics of state by selecting a specific set of sampling points. These sample points completely capture the covariance and prior mean of the state x_k, and ensure that the post-mean and post-covariance of x_{k+1} are accurately captured to the 3rd order when propagating through the nonlinear systemf_k^d.

Assume the following transformation

$$y = h(x) \tag{14}$$

By the nonlinear transformation h, the random variable y to be estimated is related to the random variable $\tilde{x}(\bar{x}, P_x)$, which represents a random variable x having a mean $\bar{x}$ and a covariance P_x. From this, a consistent estimate of y having a mean y and a covariance P_y is calculated.

The UT method fully uses the set of sigma points ς, which composed of $2n_x + 1$ pre-designed vectors and their associated weights to estimate the mean y and covariance P_y of y. The set of sigma points ς should be constructed by capturing the information (e.g., the mean and covariance) of the random input variable x (Julier et al., 2000).

One of the ways to construct the set of sigma points ς is following

$$\begin{cases} X^{(0)} = \bar{x} & W^{(0)} = w^{(0)} \\ X^{(i)} = \bar{x} + \left(\sqrt{\frac{n_x}{1-W^{(0)}} P_x}\right)_i & W^{(0)} = \frac{1-w^{(0)}}{2n_x} \\ X^{(i+n_x)} = \bar{x} - \left(\sqrt{\frac{n_x}{1-W^{(0)}} P_x}\right)_i & W^{(i+n_x)} = \frac{1-w^{(0)}}{2n_x} \end{cases} \tag{15}$$

where n_x is the dimension of the random variable x, w, the weight on the mean point denotes a tuning parameter, and the operator $\sqrt{\cdot}$ is the Cholesky decomposition and $(\sqrt{\cdot})_i$ represents the i-th column of the decomposed matrix, $\mathrm{i} = 1, 2, \ldots, n_x$.

The estimate of $\tilde{y}(\bar{y}, P_y)$ is as follows,

$$\begin{cases} Y^{(j)} = h\left(X^{(j)}\right) \\ \bar{y} = \sum_{j=0}^{2n_x} W^{(j)} \cdot Y^{(j)} \\ P_y = \sum_{j=0}^{2n_x} W^{(j)} \cdot \left(Y^{(j)} - \bar{y}\right) \cdot \left(Y^{(j)} - \bar{y}\right)' \end{cases} \tag{16}$$

2.5 The interval estimation

Generally, we use point estimation to find the unknown parameters of interest. However, in many cases, it seems desirable to obtain the upper limit and lower limit of the point estimate after a point estimate. Instead of estimating the true value as a point, we can infer that the true value of the estimated parameter is contained in a certain interval, which is the interval estimation (Mood et al., 1974).

In general, estimates are usually given in the form of the estimate with a positive or negative certain amount. For a Gaussian density, the estimate x is approximated by a Gaussian random variable given the first two moments, that is $x \sim \mathcal{N}(\bar{x}, \sigma)$.

And the interval estimate is

$$P\left[\bar{x} - \sigma Z_{1-\frac{a}{2}} < x < \bar{x} + \sigma Z_{1-\frac{a}{2}}\right] = \alpha, \alpha \in [0,1] \tag{17}$$

$\left[\bar{x} - \sigma Z_{1-\frac{a}{2}} < x < \bar{x} + \sigma Z_{1-\frac{a}{2}}\right]$, which is called confidence interval, and it covers the unknown true estimate x, which is $100\alpha\%$ (α is a confidence coefficient).

For state estimation problems, the unscented transformation described in Sec. 2.4 is applied to estimation the state $x_k \sim \mathcal{N}(\hat{x}_k, P_k)$.

In state $x_k \sim \mathcal{N}(\hat{x}_k, P_k)$ under the Gaussian assumption, as introduced in Sec 2.6, the confidence interval of each elements of the state x_k is

$$\left[\hat{x}_{i,k} - P_{ii,k} Z_{1-\frac{a}{2}}, \hat{x}_{i,k} + P_{ii,k} Z_{1-\frac{a}{2}}\right] \tag{18}$$

where $\hat{x}_{i,k}$ and $P_{ii,k}$ represent the i-th element of the state x_k and the i-th diagonal element of the error covariance P_k, respectively, and $Z_{1-\frac{a}{2}}$ is obtained by the two-tail table of Gaussian distribution once α is determined. In our simulation, the exact value of $\hat{x}_{i,k}$ and $P_{ii,k}$ at each time step k can be obtained

by UT method. Substitute the values in (18) and the coordinate transformation (10) can then be applied to calculate the envelope of the trajectory prediction.

2.6 Ideal truth and practical truth

In trajectory simulation, two different types of real trajectories are usually encountered: ideal truth and practical truth. The ideal truth is generated by (1)– (3) without any error, which means that the initial state of the dropped cylinder is known. The trajectory in this case is a deterministic process, not a random process. However, in reality, the exact initial state cannot be known, only a range of initial states containing errors can be known. In this case, the initial state is modeled as a random variable with some known distribution. Naturally, the primary choice of the distribution is the Gaussian distribution, which is the most likely initial state we think, and the covariance is the error from the disturbance, separately. Note that the UT method provides a suboptimal way for predicting the practical truth, which has been widely used in electrical engineering (Wan and Merwe, 2000).

In this thesis, we simulated both the ideal truth and the practical truth in each case and compare our prediction trajectory with these two truths to help people understand the difference directly. For example, when drop angle is 45°, the initial state of ideal truth is

$$x_0^{IT} = \left[0\ m/s, 0\ m/s, 0\ rad/s, \frac{\pi}{4} rad\right],$$

and the initial state of practical truth is one realization of the following Gaussian distribution ${x_0}^{PT} \sim \mathcal{N}(\bar{x}_0, P_0)$

where

$$\bar{x}_0 = \left[0\ m/s, 0\ m/s, 0\ rad/s, \frac{\pi}{4} rad\right],$$

$$P_0 = \mathrm{diag}\left[10^{-4}\ m^2/s^2, 10^{-4}\ m^2/s^2, \left(\frac{\pi}{90}\right)^2\ rad^2/s^2, \left(\frac{\pi}{90}\right)^2\ rad^2/s^2\right],$$

The propagation of two different initial states is governed by the dynamic model (11). This can result in the trajectories of ideal truth and practical truth, respectively.

III. Case Study

3.1 Properties of dropped cylinders

Table 1 shows the characteristics of the dropped cylinder. They were freely dropped from the calm water surface in the experimental tests (Aanesland, 1987). In the numerical analysis, it is also assumed that they freely fall into the water. More details on the experimental tests can be found in (Aanesland, 1987).

Table 1 Properties of scaled dropped cylinders

Parameters	Unit	Full Scale	Model Scale (1:20:32)
Length (L)	m	9.95	0.45
Mass density (ρ_c)	kg/m	225	0.548
Diameter (D)	m	0.203	0.01

3.2 Force components analysis for drop angle 45°

Firstly, the force component in the x direction consists of two parts, the frictional drag (F_{dx1}) and the form drag (F_{dx2}). As can be seen from Figure 2, the form drag dominates at the beginning, but decays rapidly over time. The transient part almost vanishes after 17s around, and steady state part becomes more and more obvious. In the steady state, the frictional drag is still smaller than the form drag, which means that, the form drag F_{dx2} is the main component in this example.

The calculation of the force F_{dz} in the z direction is based on the Morison equation. Only the drag term is retained here. The magnitude of F_{dz} rises sharply after entering the water, and it becomes periodic after two cycles. The pitch moment M_{dy} shows very similar pattern with F_{dz}, which is indicated by equations (5) and (6).

It should be noted that in our current discussion we have ignored the impact of water-entry.

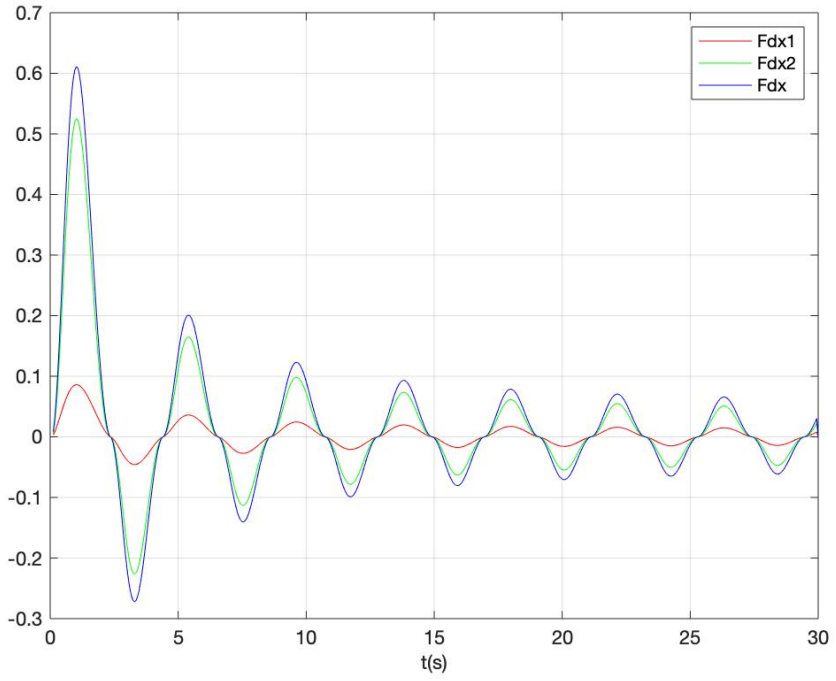

Figure 2 Surge force at drop angle 45°

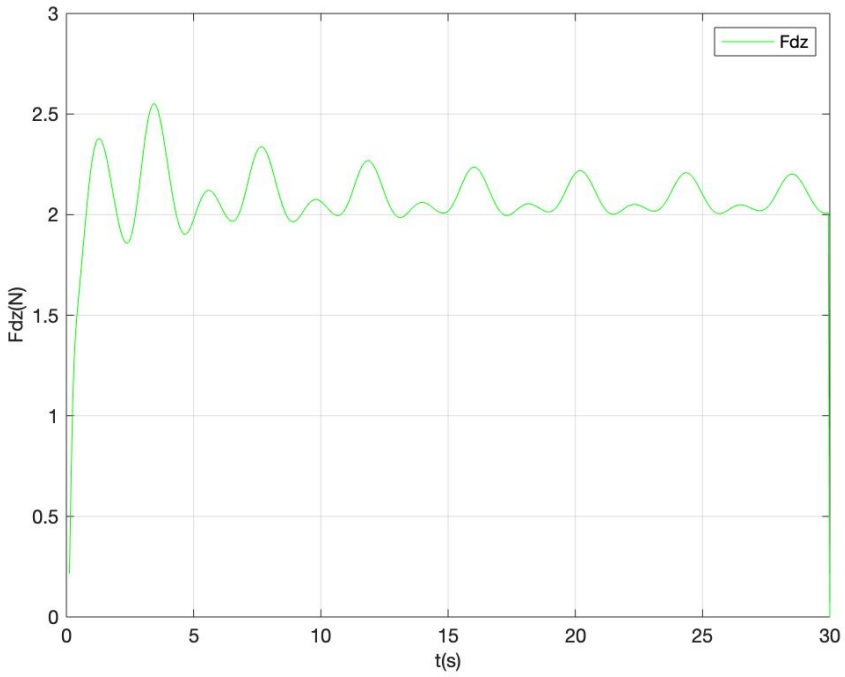

Figure 3 Heave force at the drop angle 45°

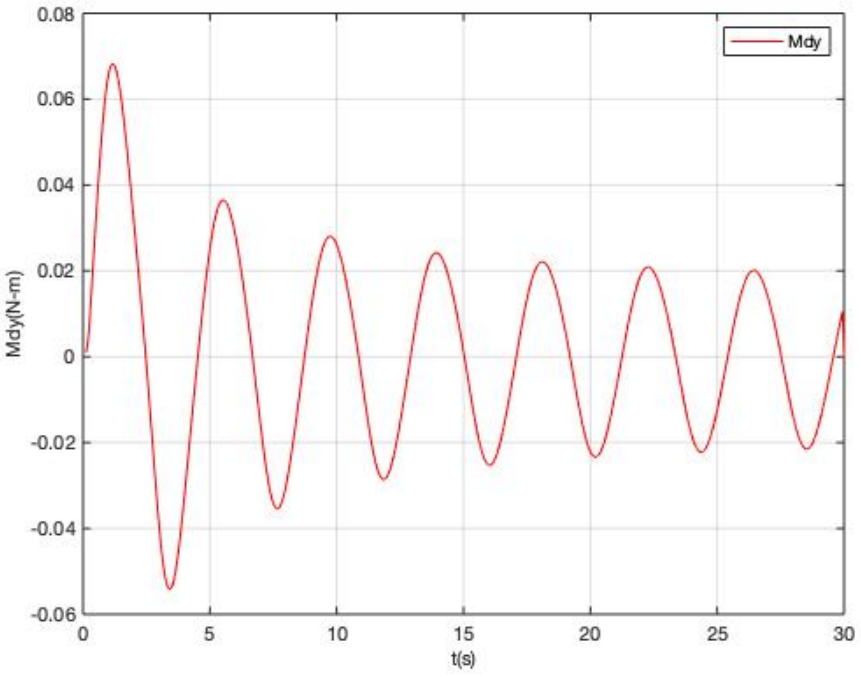

Figure 4 Pitch moment at the drop angle 45°

3.3 Performance parameters R_A and R_L for drop angle 45°

In Sec. 2.2, the state space model of the dropped cylinder is successfully constructed. As mentioned earlier, the entire process is random, and this model provides us a convenient way to consider the effects of random noise. The results obtained by the MC and UT methods are shown below. First, consider the case where the drop angle is 45 °. In Figure 5, the black, red, and green solid line represent the ideal truth, practical truth and predicted trajectory from the MC method, respectively. The green dash line and the green dash-dot line represent the upper limit (UL) and lower limit (LL) of the MC method, respectively. The blue dash line and the blue dash-dot line represent the upper limit (UL) and lower limit (LL) of the experimental test, respectively.

In Figure 5, the result corresponds to the MC method based on 256 samples, the sigma range is equal to 1, and the drop angle is 45 °. Those results under other different conditions can be found in the Appendix. In general, the trajectory (green line) predicted by the MC method is very close to ideal truth (black line) and practical truth (red line). In Figure 6, the "cyan" shaded area is the overlapping area A_{olp} between the predicted drop range from the MC method and the experimental envelope which covers the area A_{ee}. Here, a new performance parameter is proposed, namely the ratio of the overlap area A_{olp} to the experimental envelope area A_{ee}, as shown below

$$R_A = \frac{A_{olp}}{A_{ee}} \tag{19}$$

The above ratio R_A can be used to measure the quality of numerical results which are compared with the experimental data. Usually, when R_A is greater than 0.5, it is considered that the area of coincidence is large, and the probability of occurrence is also large. Further, the other performance parameter, R_L, can be proposed in a similar way, and it is the ratio between the overlap length $L_{olp}$and the experimental envelope L_{ee} at the bottom, that is

$$R_L = \frac{L_{olp}}{L_{ee}} \tag{20}$$

It can be used to measure the accuracy of the probable range at the bottom, if compared with the experimental data.

Similarly, the above parameters are also applied to evaluate the results of the UT method, as shown in Figures 7 and 8. Compared with the results of the MC method, the trajectory (green line) predicted by the UT method in this case is closer to the ideal truth (black line) and practical truth (red line). In addition, the overlap area A_{olp} and the overlap length L_{olp} from these two methods are very close. This means that, the results obtained by the two methods are not significantly different.

For the drop angle of 45 °, R_A and R_L calculated by the two methods under different conditions have been summarized in Tables 2 and 3, respectively. Corresponding to different samples, the results from the MC method are shown in Table 2. With the increase of the number of samples, the calculation time also increases significantly, and both R_A and R_L do not change too much if the sample is more

than 81. However, as shown in Figure 9, the calculation time increases exponentially with the number of samples. It can be seen that the application of the MC method requires a large number of samples to obtain relatively accurate results. Increasing the number of samples is not an effective way to improve accuracy.

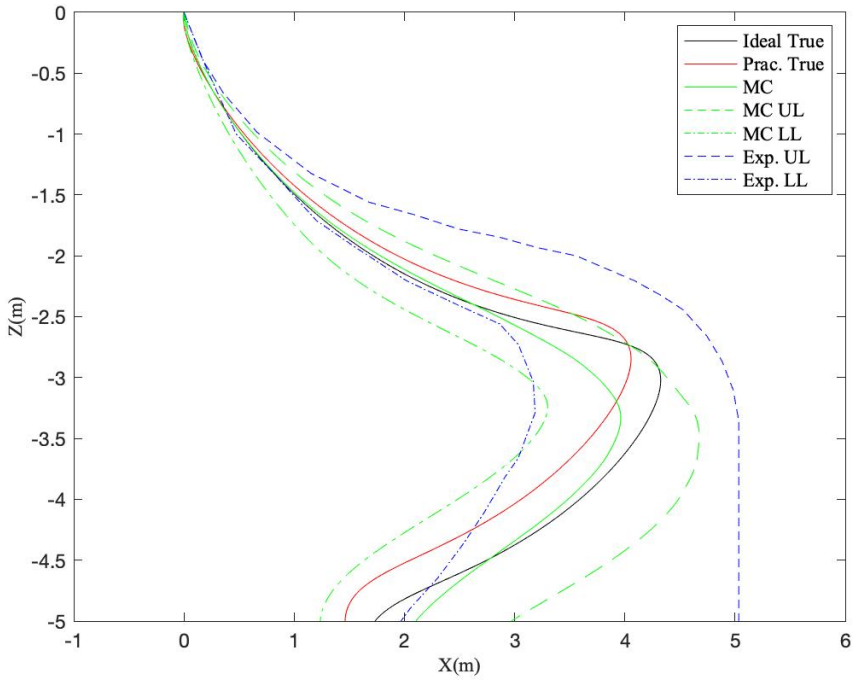

Figure 5 Trajectory prediction at the drop angle $45°$ using MC method (Samples =256, sigma range =1)

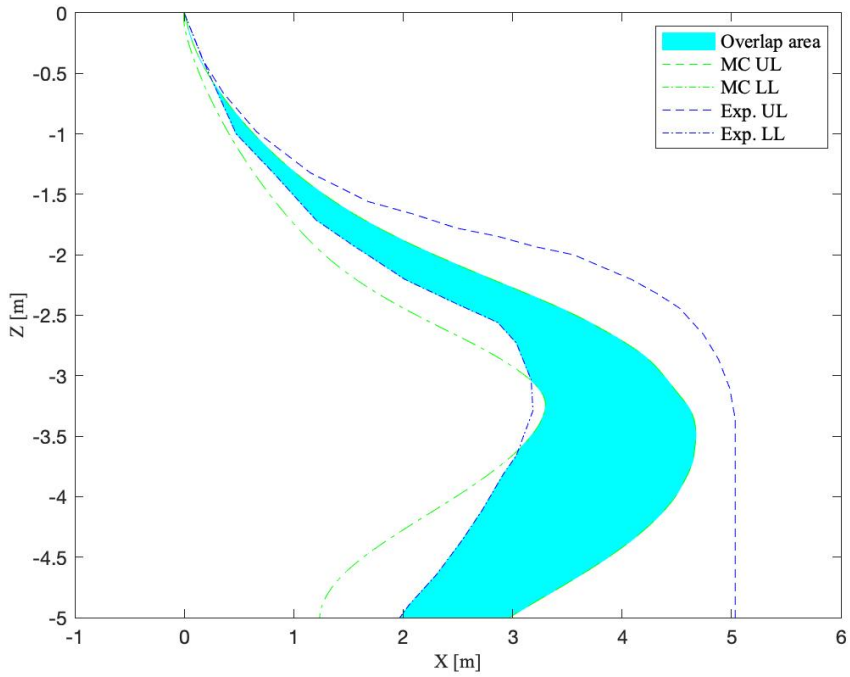

Figure 6 Overlap area between MC method and experimental envelope with the drop angle 45°(Samples =256, sigma range =1)

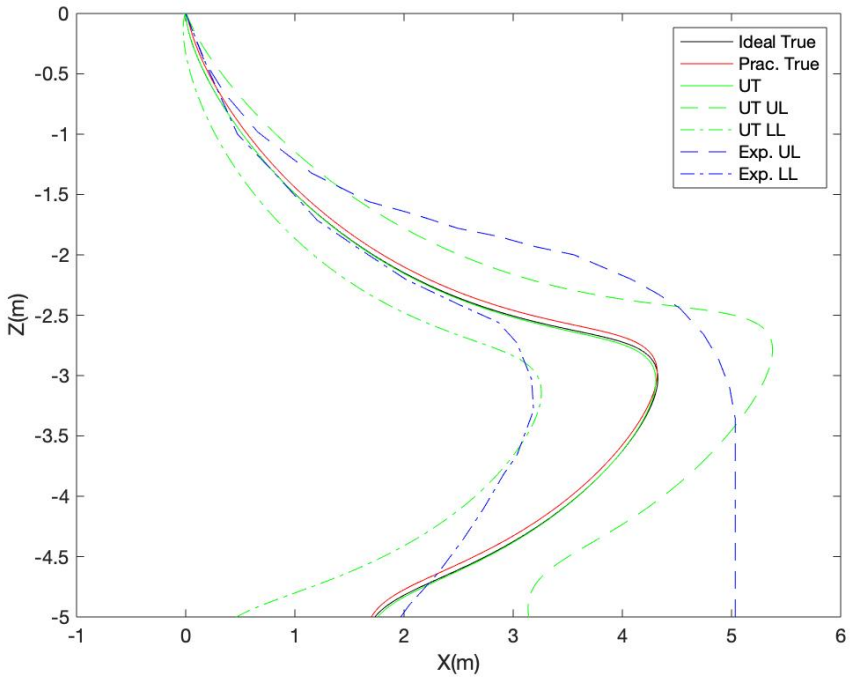

Figure 7 Trajectory prediction at the drop angle 45° using UT method (Probability=0.6826)

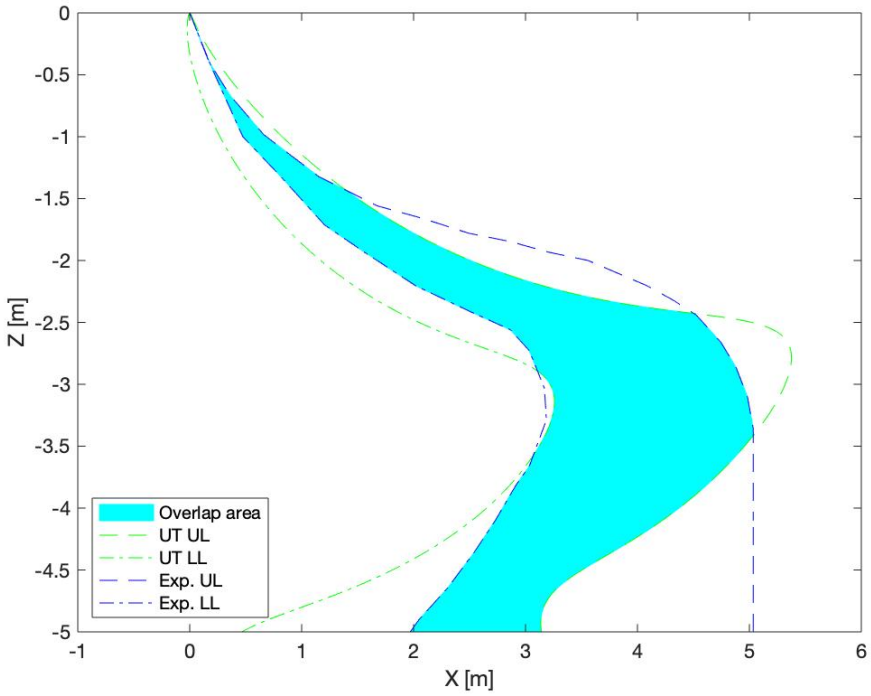

Figure 8 Overlap area between UT method and experimental envelope with the drop angle 45°(Probability=0.6826)

Table 2 Prediction results derived from MC method at drop angle=45° (Sigma range=1)

Samples	Time(s)	R_A	R_L
$2^4 = 16$	2.089	0.518	0.145
$3^4 = 81$	10.326	0.566	0.323
$4^4 = 256$	49.843	0.572	0.326
$5^4 = 625$	123.078	0.565	0.319
$6^4 = 1296$	241.204	0.579	0.348
$7^4 = 2401$	433.816	0.579	0.345
$8^4 = 4096$	526.301	0.581	0.355
$9^4 = 6561$	856.669	0.584	0.359

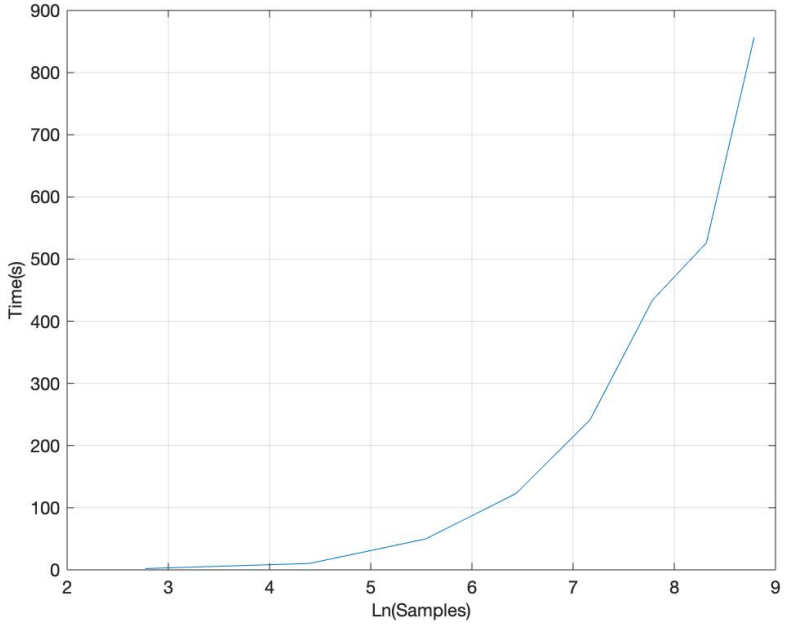

Figure 9 Time(s) vs. Ln(Sample) from MC method for drop angle 45°

In Table 3, the calculation time based on the UT method with different probability is not significantly different, and it's much smaller than the calculation time using the MC method. Table 4 lists the different results obtained by the two methods under the same conditions. It can be seen that the difference between their R_A and R_L is not large, but the time required by the UT method is only 3% of the MC method.

Table 3 Prediction results derived from UT method at drop angle=45° (Probability=0.1- 0.9)

P	Time(s)	R_A	R_L
0.1	1.943	0.104	0.000
0.2	1.862	0.204	0.038
0.3	1.892	0.306	0.095
0.4	1.859	0.412	0.157
0.5	1.860	0.514	0.226
0.6	1.917	0.613	0.305
0.7	1.889	0.708	0.401
0.8	1.853	0.788	0.527
0.9	1.872	0.884	0.729

Table 4 Prediction results derived from these two methods under the same conditions at drop angle= 45°

Method	P	Sigma range	Time(s)	R_A	R_L
MC(Samples=256)	0.6826	1	49.843	0.572	0.326
UT	0.6826	1	1.737	0.693	0.382

IV. Conclusions

In this thesis, the state space model has been successfully constructed to investigate the stochastic behavior of the cylinders falling into water in two dimensions using two different statistical methods, i.e., MC method and UT method. MC method is the most well-known method for solving stochastic problems, and UT method is widely used for the parameter estimation and the state estimation.

In general, MC method is reliable under the premise of a large number of samples. According to the case study above, the results obtained by the UT method behaves similar to MC method with reasonable sample size. However, by comparing the trajectory accuracy and computation time between these two methods, our results show that the UT method has better tradeoff between the accuracy and the computation requirement in the case of cylinders that fall into water freely. Therefore, when solving similar problems, we recommend using UT method instead.

Reference

Aanesland, V., 1987. Numerical and experimental investigation of accidently falling drilling pipes. In: Offshore Technology Conference.

ABS, 2013. Guidance Notes on Accidental Load Analysis and Design for Offshore Structures.

Anderson, B.D.O., Moore, J.B., 1979. Optimal Filtering. Prentice Hall, Englewood Cliffs, NJ.

Awotahegn, M., 2014. Experimental Investigation of Accidental Drops of Drill Pipes and Containers. Master's thesis. University of Stavanger.

Colwill, A., Ahilan, A., 1992. Reliability analysis of the behavior of dropped objects. In: Offshore Technology Conference.

der Merwe, R.V., Wan, E.A., 2001. The square-root unscented kalman filter for state and parameter-estimation. In: IEEE International Conference on Acoustics, Speech, and Signal Processing. Proceedings, 2001.

DNV, 2010. Risk Assessment of Pipeline Protection. DNV-RP-F107.

Hoerner, S., 1965. Fluid-Dynamic Drag. Hoerner Fluid Dynamics.

Ito, K., Xiong, K., May 2000. Gaussian filters for nonlinear filtering problems. IEEE Trans. Autom. Control 45 (5), 910–927.

Julier, S.J., Uhlmann, J.K., 1997. A consistent, debiased method for converting between polar and cartesian coordinate systems. In: Proceedings of SPIE Acquisition, Tracking, and Pointing XI, 3086.

Julier, S., Uhlmann, J., Durrant-Whyte, H.F., March 2000. A new method for the nonlinear transformation of means and covariances in filters and estimators. IEEE Trans. Autom. Control 45 (3), 477–482.

Katteland, L., Øygarden, B., 1995. Risk analysis of dropped objects for deep water development. In: The International Conference on Offshore Mechanics and Arctic Engineering. American Society of Mechanical Engineers, pp. 443–450.

Luo, Y., Davis, J., 1992. Motion simulation and hazard assessment of dropped objects. In: International Offshore and Polar Engineering Conference.

Mendel, J.M., 1995. In: Oppenheim, A.V. (Ed.), Lessons in Estimation Theory for Signal Processing, Communications, and Control, second ed. Prentice Hall, Mar.

Menegaz, H.M.T., Ishihara, J.Y., Borges, G.A., Vargas, A.N., Oct. 2015. A systematization of the unscented Kalman filter theory. IEEE Trans. Autom. Control 60, 2583–2598.

Meng, H., Li, X.R., Jilkov, V.P., jul 2018. Optimized Gauss-Hermite quadrature with application to nonlinear filtering. In: 2018 21st International Conference on Information Fusion (FUSION). IEEE.

Mood, A.M., Graybill, F.A., Boes, D.C., 1974. Introduction to the Theory of Statistics, Ser. McGraw-Hill Series in Probability and Statistics. McGraw-Hill Companies.

Newman, J.N., 1977. Marine Hydrodynamics. The MIT Press.

Schlichting, H., 1979. Boundary Layer Theory. McGraw-Hill Book Company.

Wan, E., Merwe, R.V.D., Oct. 2000. The unscented kalman filter for nonlinear estimation. In: Proceedings of the IEEE 2000 Adaptive Systems for Signal Processing, Communications, and Control Symposium.

Xiang, G., Birk, L., Li, L., Yu, X., Luo, Y., 2016. Risk free zone study for cylindrical objects dropped into water. Ocean Syst. Eng. 6 (4), 377–400.

Xiang, G., Birk, L., Yu, X., Lu, H., 2017. Numerical study on the trajectory of dropped cylindrical objects. Ocean Eng. 130, 1–9.

Xiang, G., Birk, L., Yu, X., Li, X., 2017. Study on the trajectory and landing points of dropped cylindrical object with different longitudinal center of gravity. Int. J. Offshore Polar Eng. 27 (3), 274–282.

Xiang, G., Li, X., Yu, X., Luo, Y., Cao, Y., feb 2019. Motion dynamics of dropped cylindrical objects in flows after water entry. Ocean Eng. 173, 659–671.

Appendix

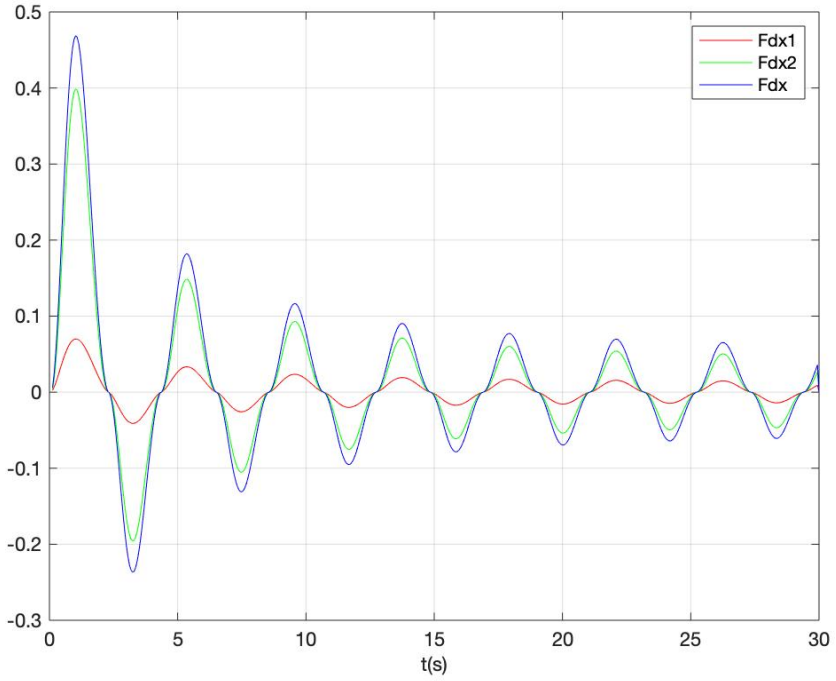

Figure 10 Surge force at drop angle 30°

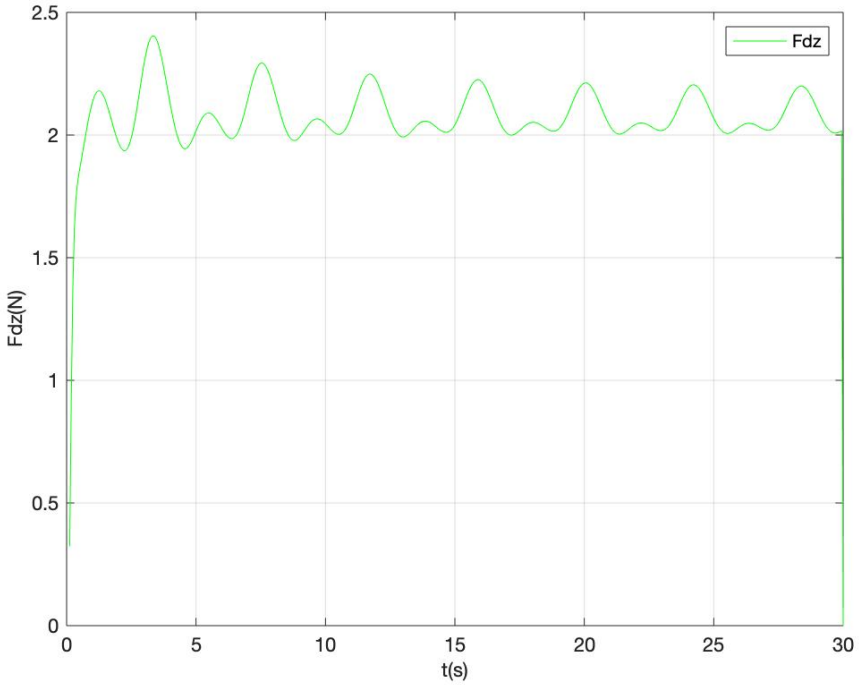

Figure 11 Heave force at the drop angle 30°

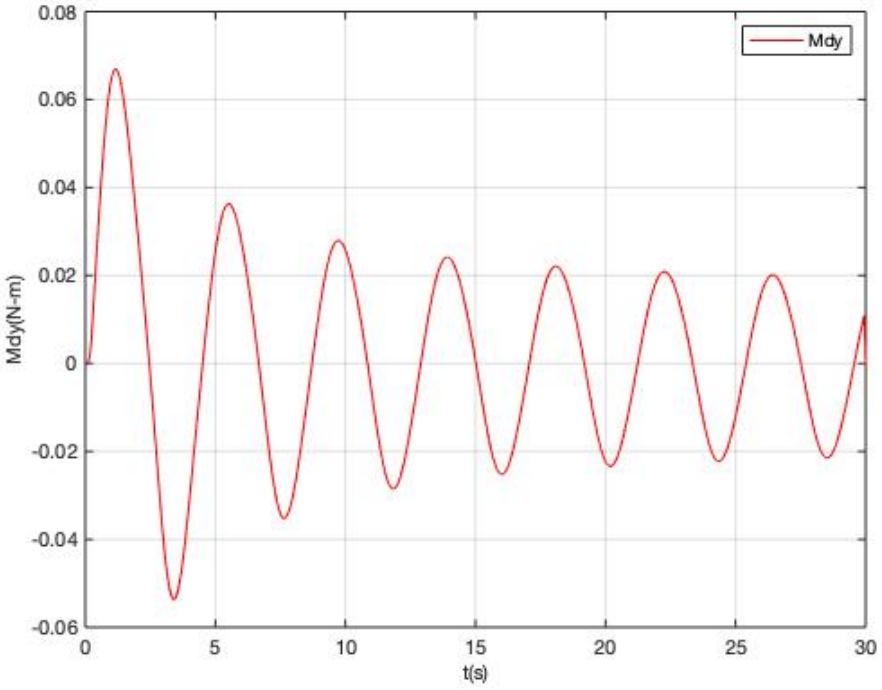

Figure 12 Pitch moment at the drop angle 30°

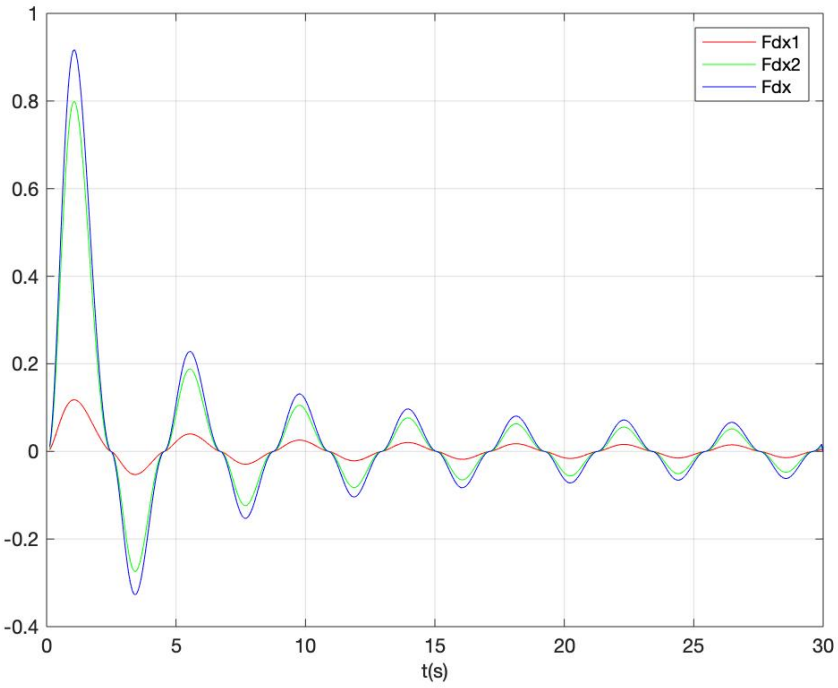

Figure 13 Surge forces at drop angle 60°

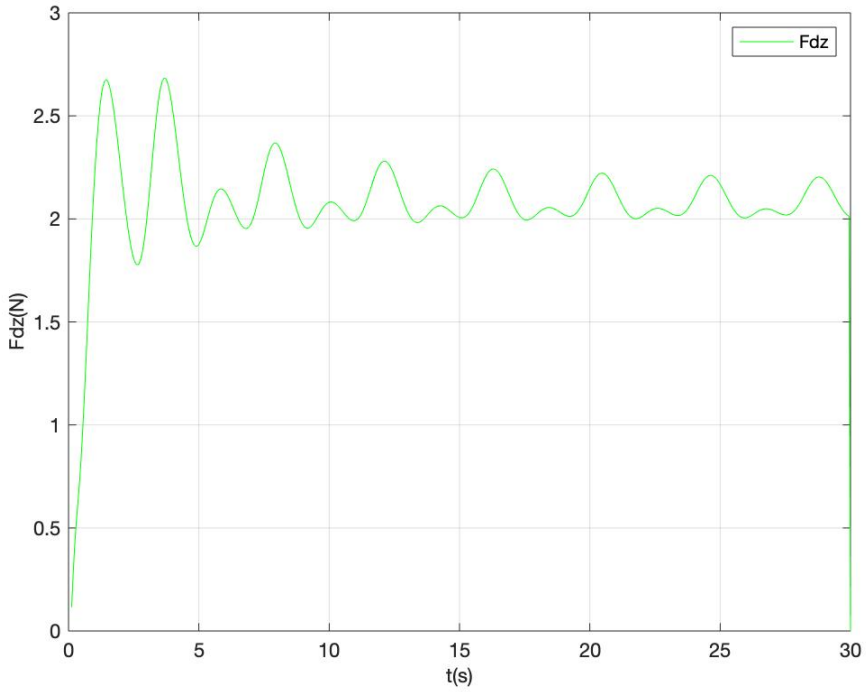

Figure 14 Heave force at the drop angle 60°

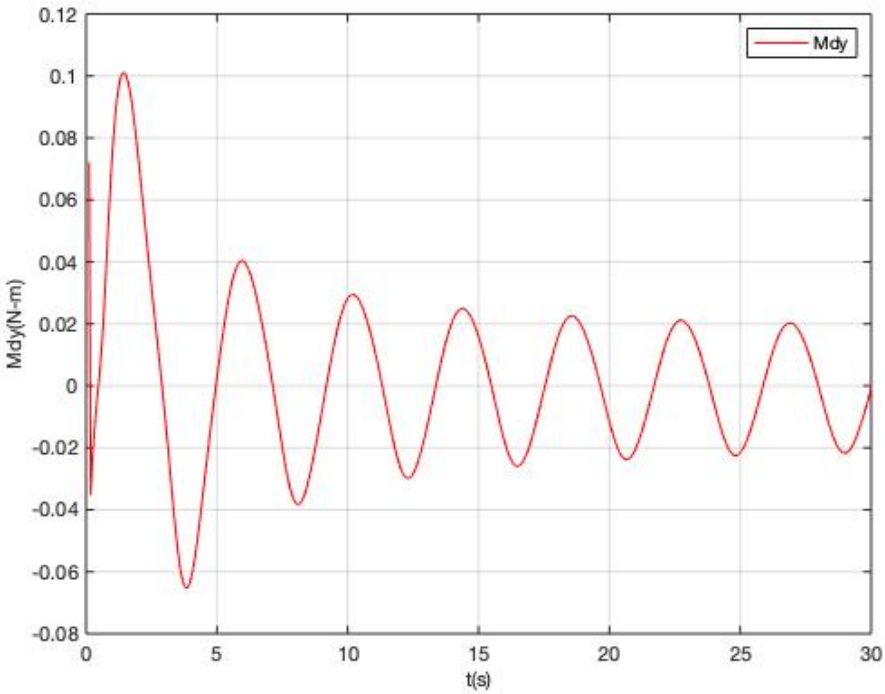

Figure 15 Pitch moment at the drop angle 60°

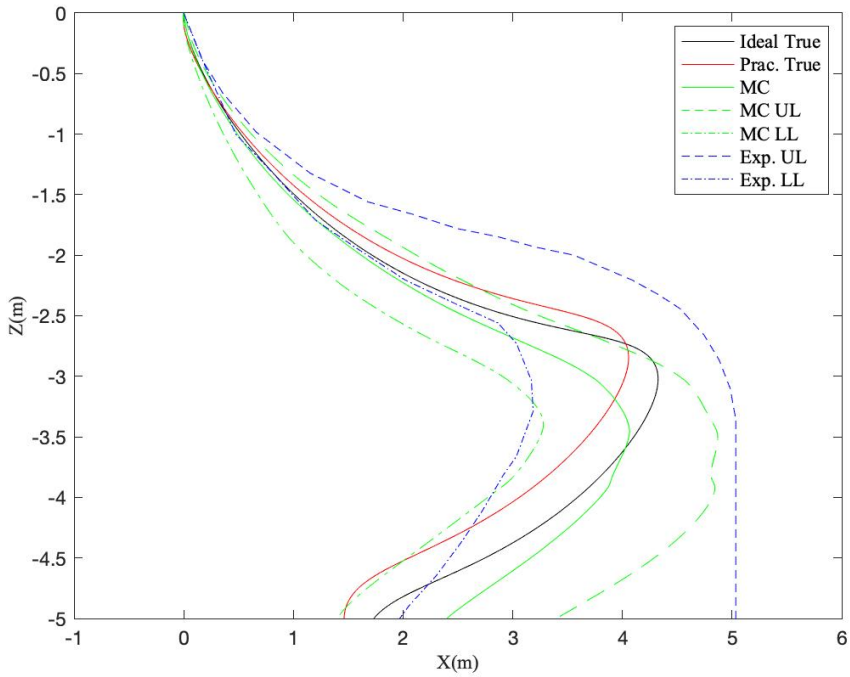

Figure 16 Trajectory prediction at the drop angle 45° using MC method (Samples =16, sigma range =1)

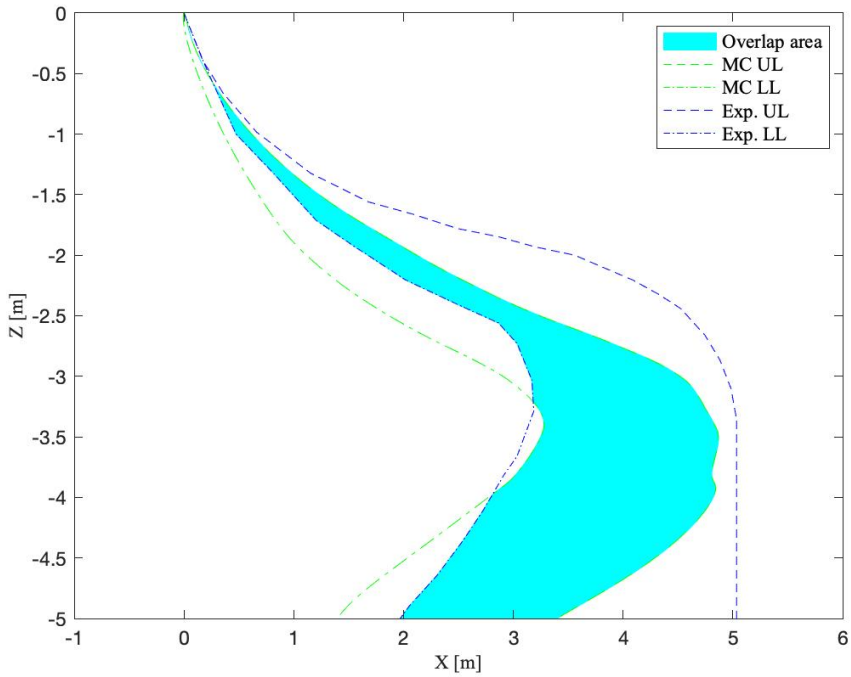

Figure 17 Overlap area between MC method and experimental envelope with the drop angle 45°(Samples =16, sigma range =1)

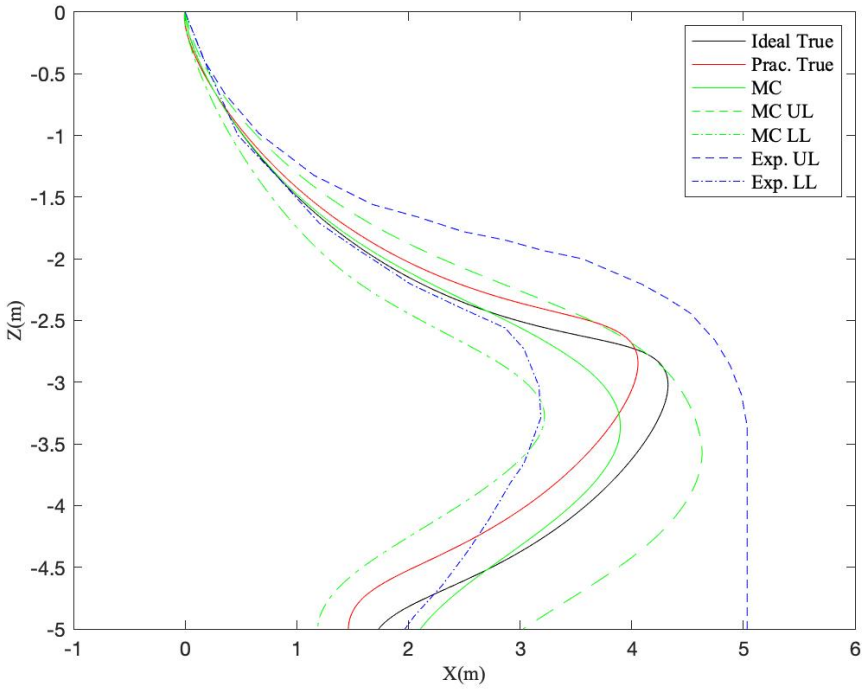

Figure 18 Trajectory prediction at the drop angle 45° using MC method (Samples =2401, sigma range =1)

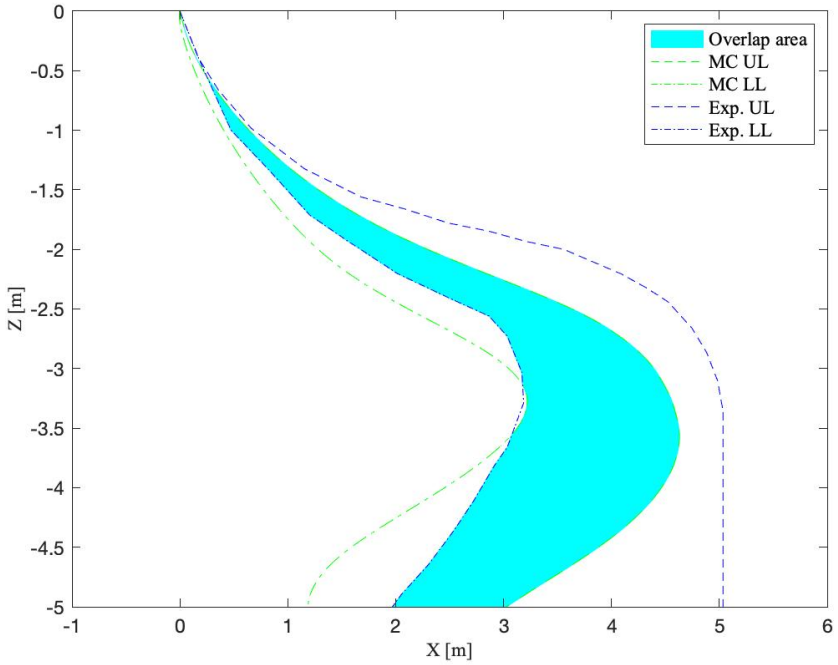

Figure 19 Overlap area between MC method and experimental envelope with the drop angle 45°(Samples =2401, sigma range =1)

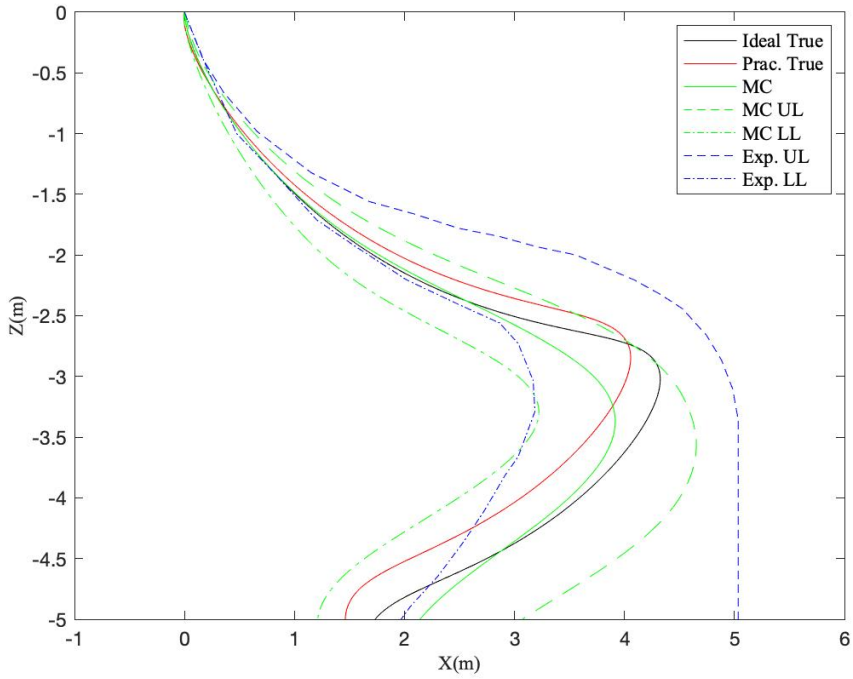

Figure 20 Trajectory prediction at the drop angle 45° using MC method (Samples =6561, sigma range =1)

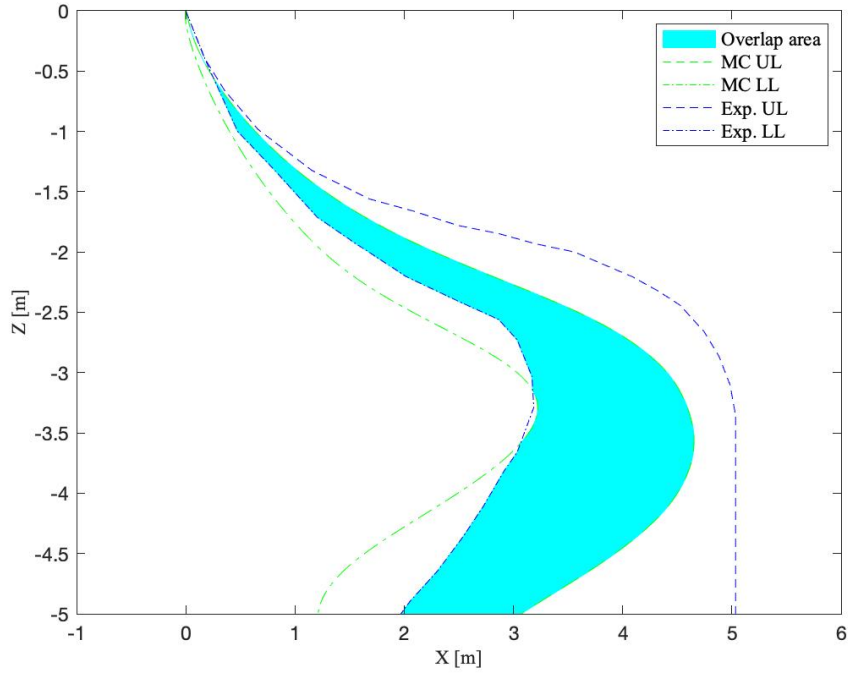

Figure 21 Overlap area between MC method and experimental envelope with the drop angle 45°(Samples =6561, sigma range =1)

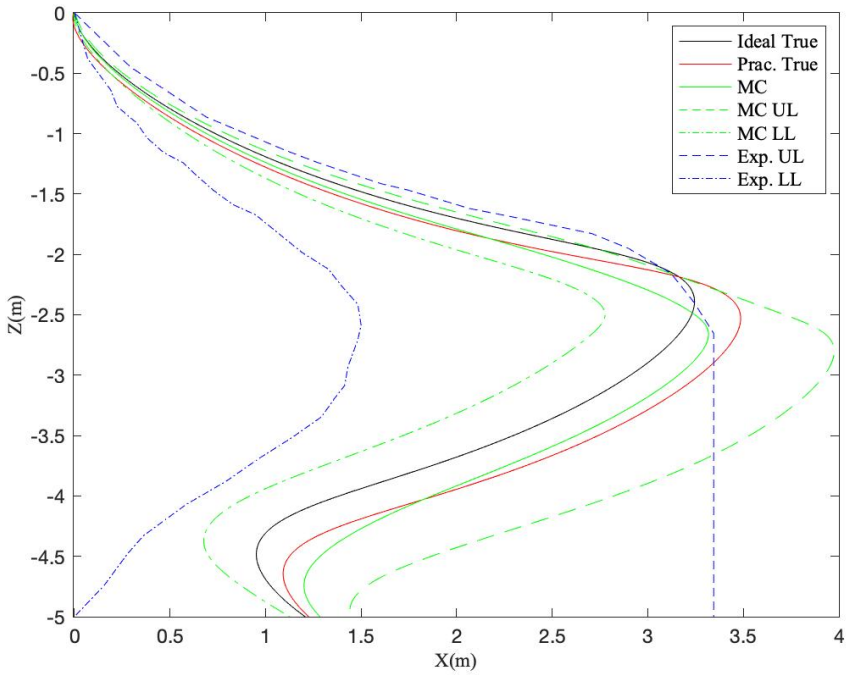

Figure 22 Trajectory prediction at the drop angle 30° using MC method (Samples =16, sigma range =1)

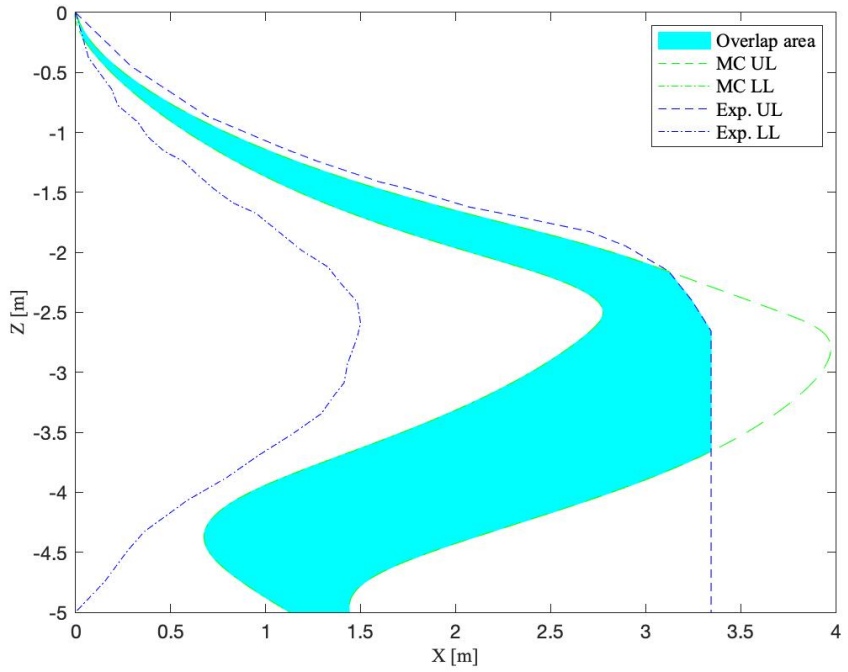

Figure 23 Overlap area between MC method and experimental envelope with the drop angle 30°(Samples =16, sigma range =1)

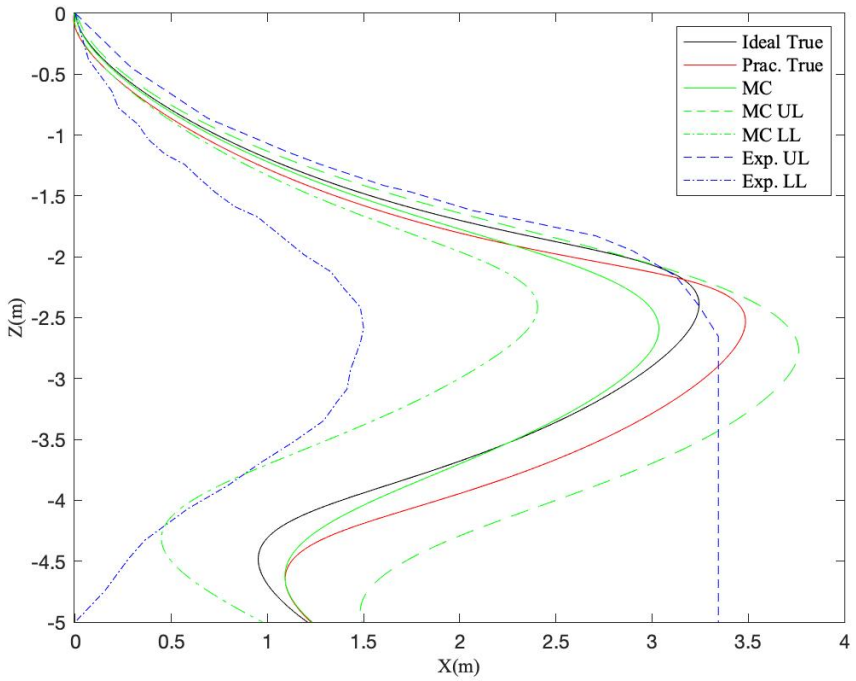

Figure 24 Trajectory prediction at the drop angle 30° using MC method (Samples =2401, sigma range =1)

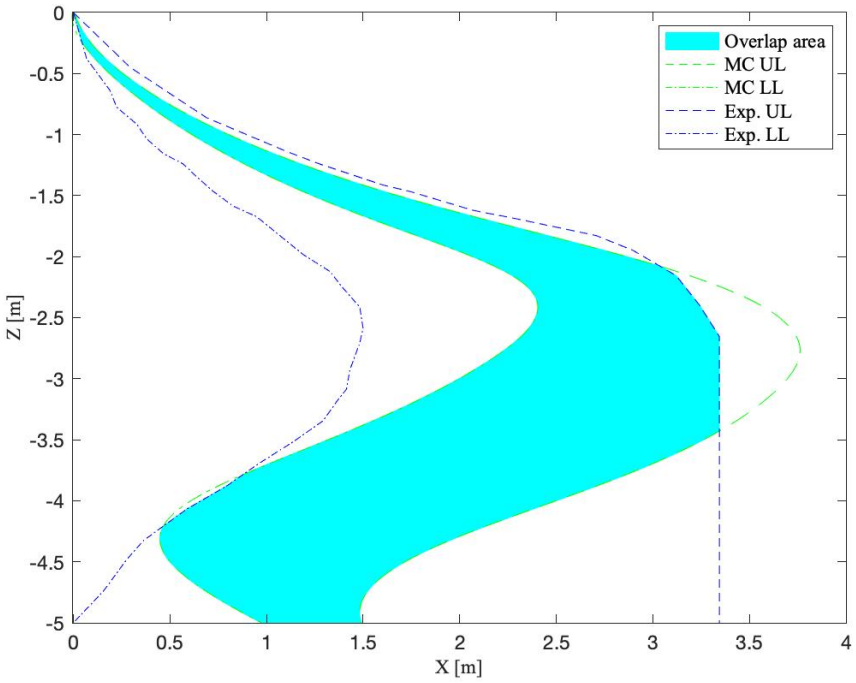

Figure 25 Overlap area between MC method and experimental envelope with the drop angle 30°(Samples =2401, sigma range =1)

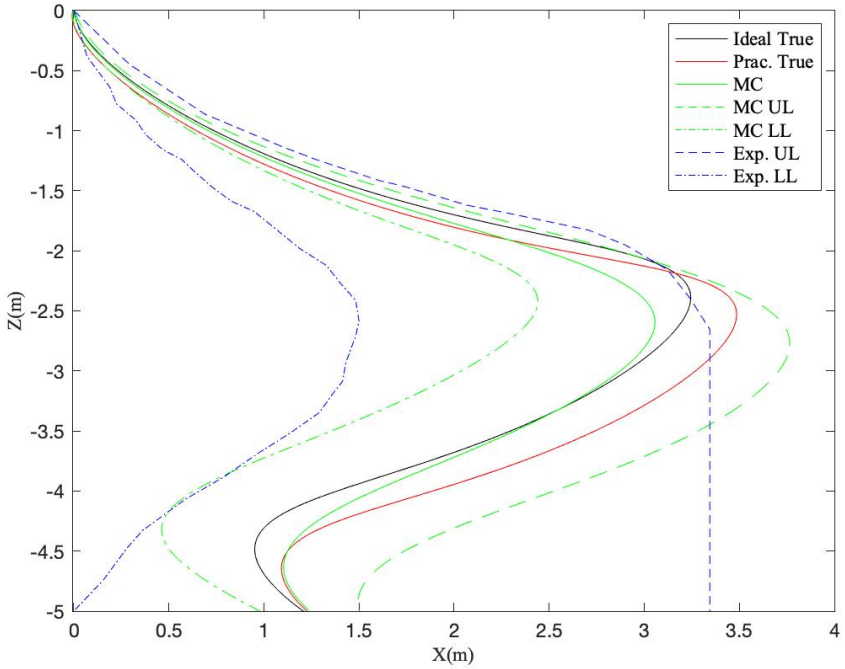

Figure 26 Trajectory prediction at the drop angle 30° using MC method (Samples =6561, sigma range =1)

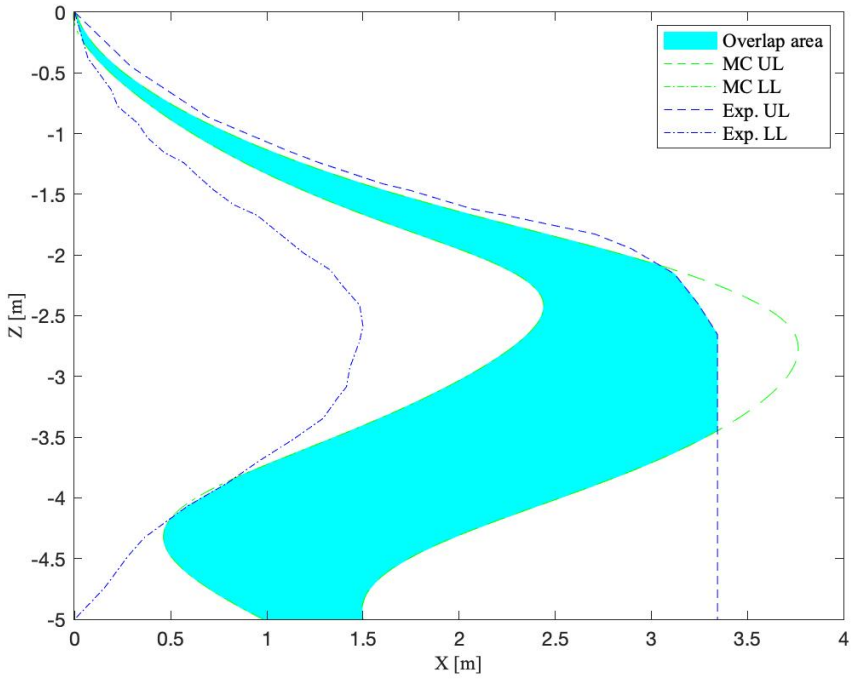

Figure 27 Overlap area between MC method and experimental envelope with the drop angle 30°(Samples =6561, sigma range =1)

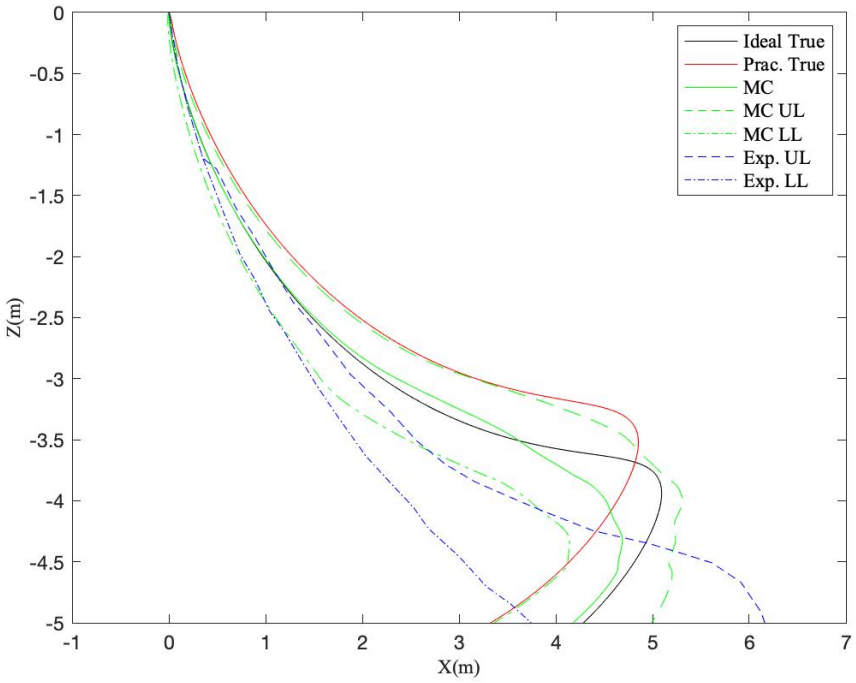

Figure 28 Trajectory prediction at the drop angle 60° using MC method (Samples =16, sigma range =1)

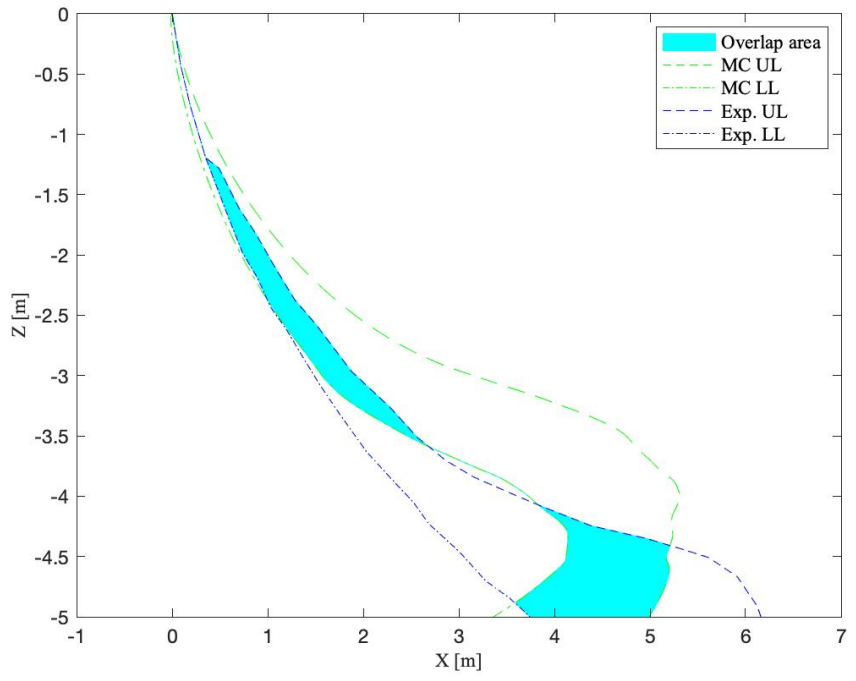

Figure 29 Overlap area between MC method and experimental envelope with the drop angle 60°(Sampling times=16, sigma range =1)

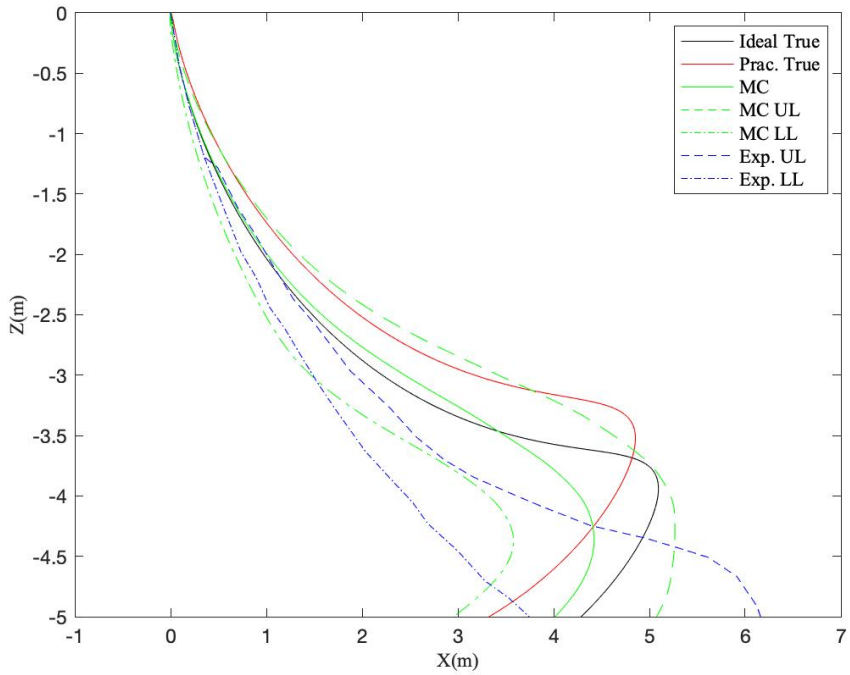

Figure 30 Trajectory prediction at the drop angle 60° using MC method (Samples =2401, sigma range =1)

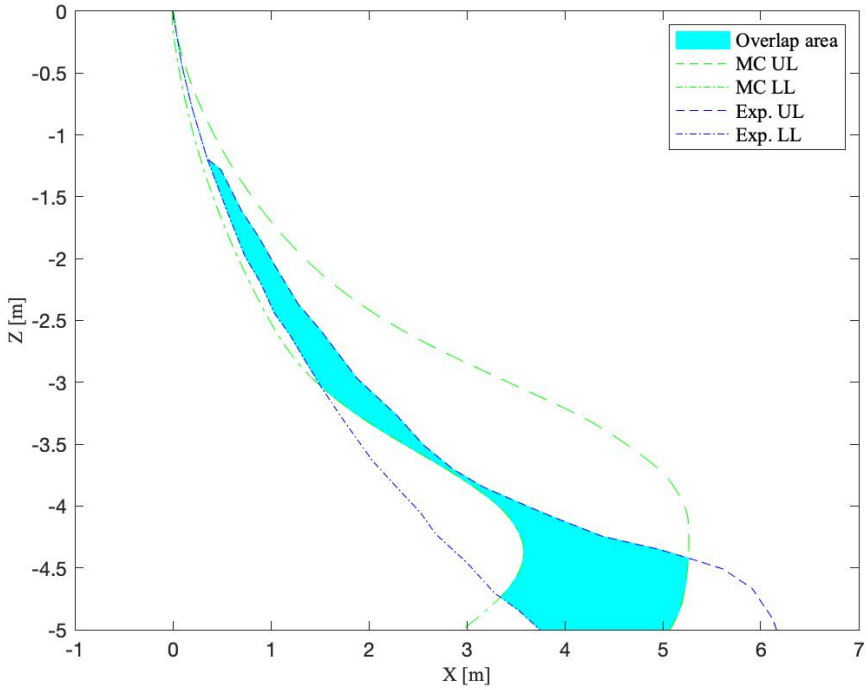

Figure 31 Overlap area between MC method and experimental envelope with the drop angle 60°(Sampling times=2401, sigma range =1)

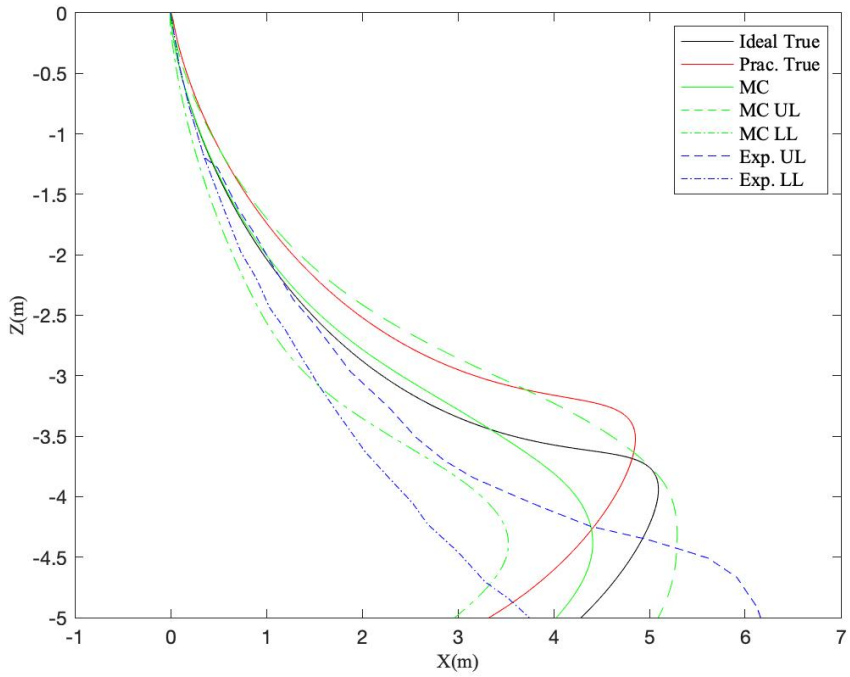

Figure 32 Trajectory prediction at the drop angle 60° using MC method (Samples =6561, sigma range =1)

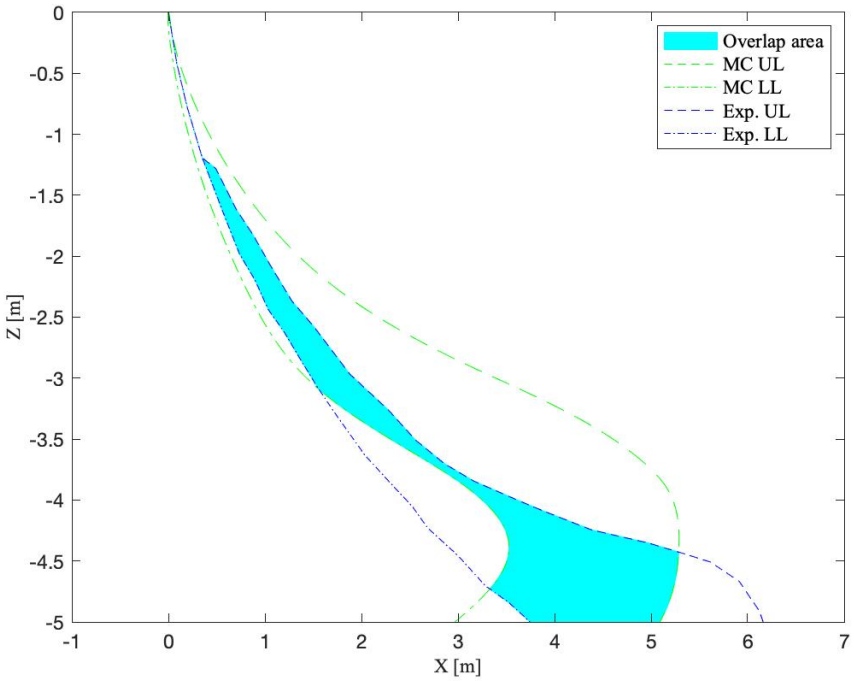

Figure 33 Overlap area between MC method and experimental envelope with the drop angle 60°(Sampling times=6561, sigma range =1)

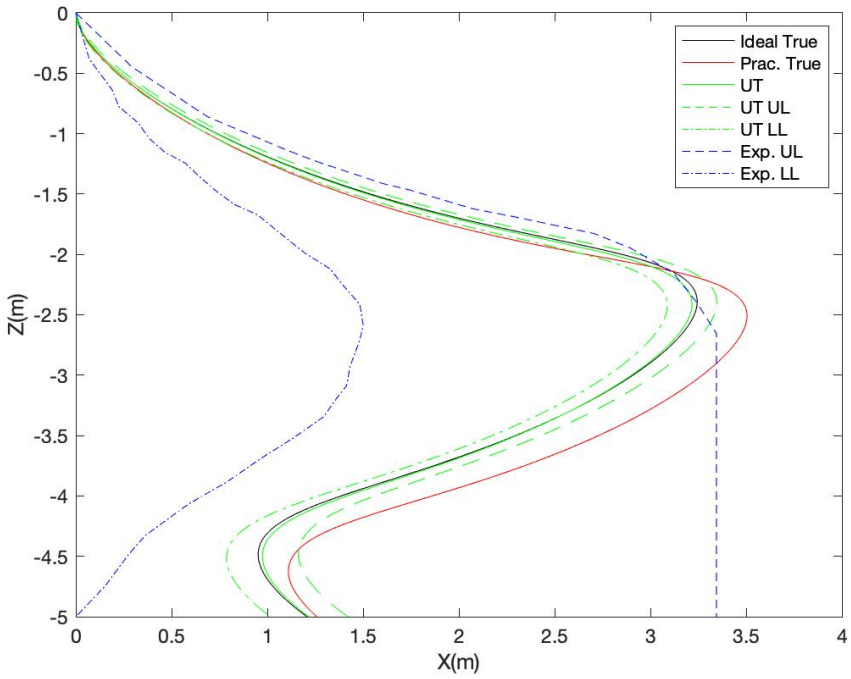

Figure 34 Trajectory prediction at the drop angle 30° using UT method(Probability=0.1)

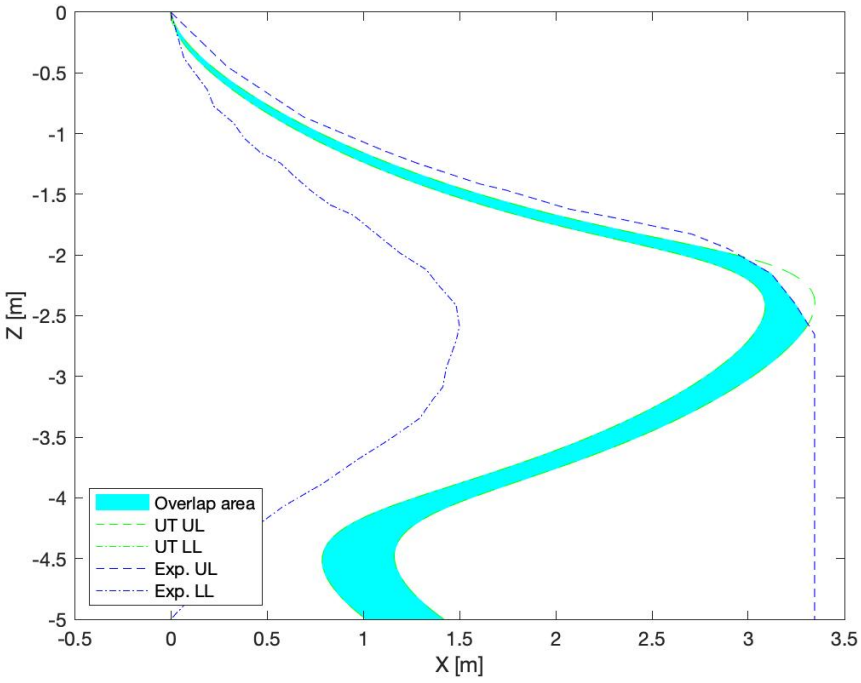

Figure 35 Overlap area between UT method and experimental envelope with the drop angle 30°(Probability=0.1)

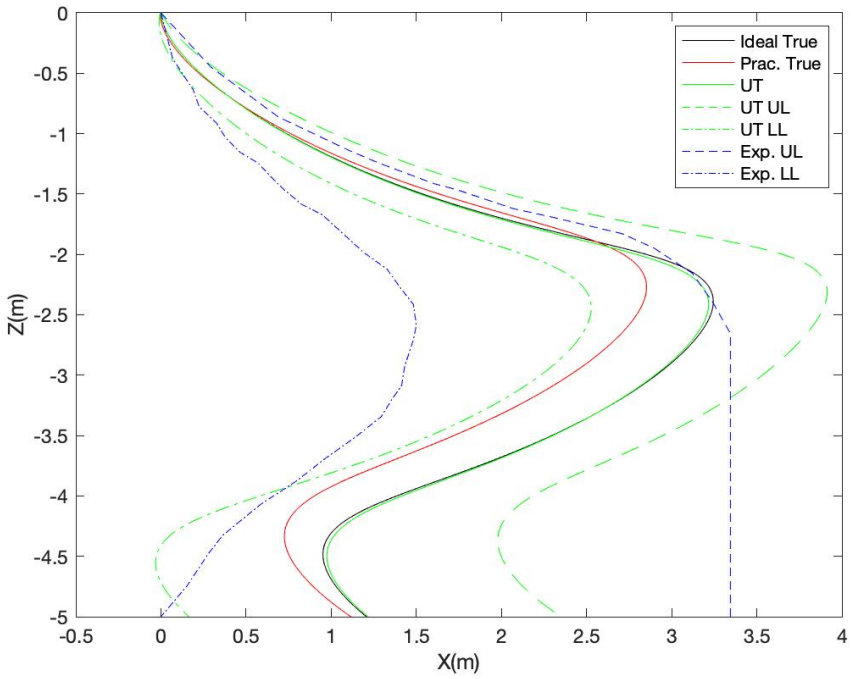

Figure 36 Trajectory prediction at the drop angle 30° using UT method (Probability=0.5)

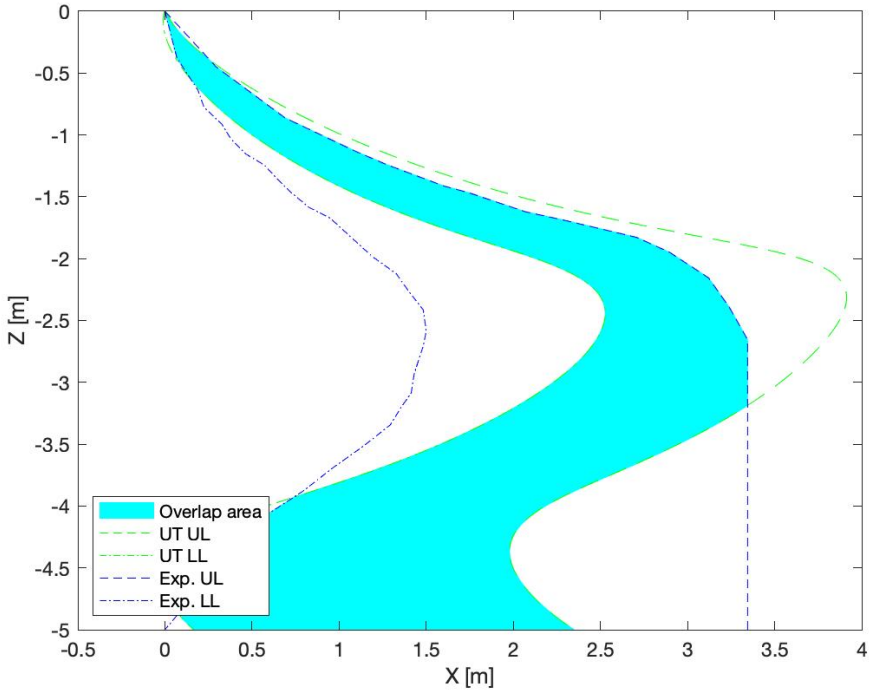

Figure 37 Overlap area between UT method and experimental envelope with the drop angle 30°(Probability=0.5)

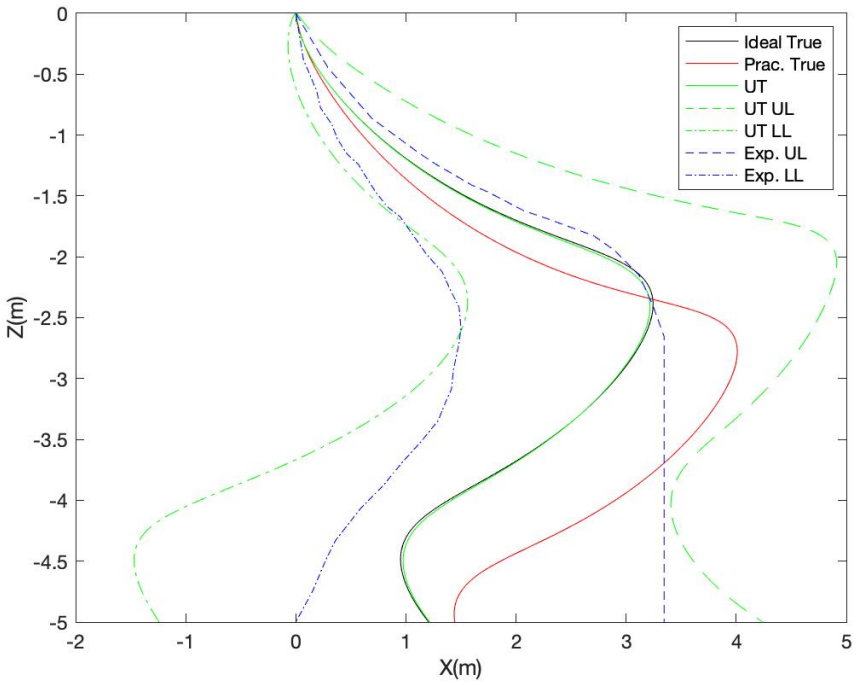

Figure 38 Trajectory prediction at the drop angle 30° using UT method (Probability=0.9)

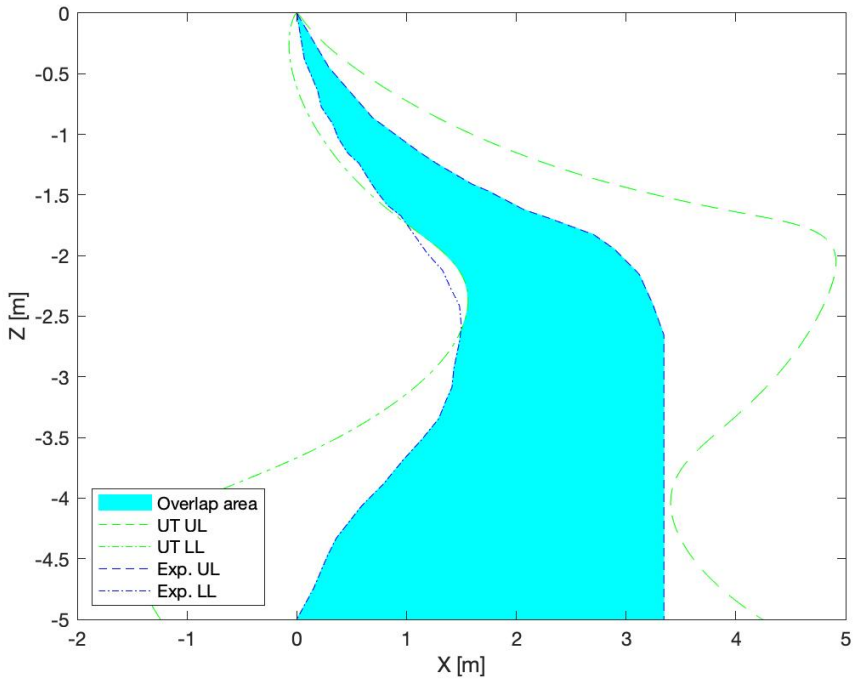

Figure 39 Overlap area between UT method and experimental envelope with the drop angle 30°(Probability=0.9)

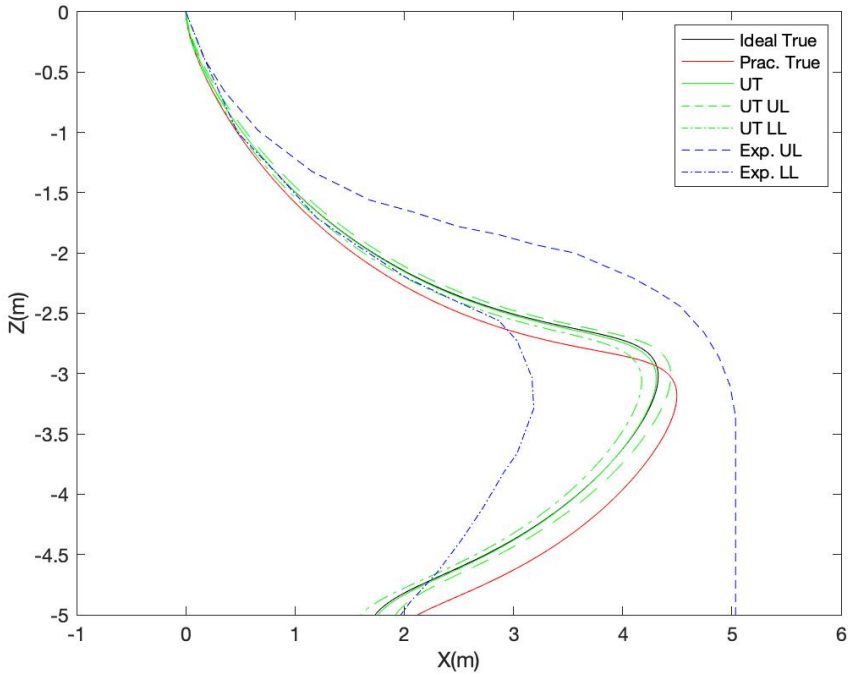

Figure 40 Trajectory prediction at the drop angle 45° using UT method (Probability=0.1)

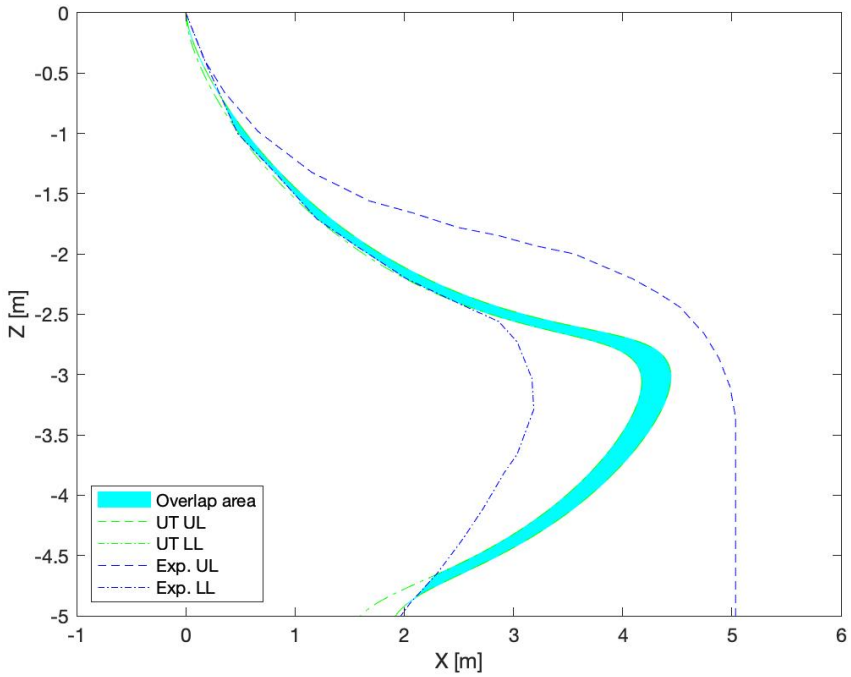

Figure 41 Overlap area between UT method and experimental envelope with the drop angle 45°(Probability=0.1)

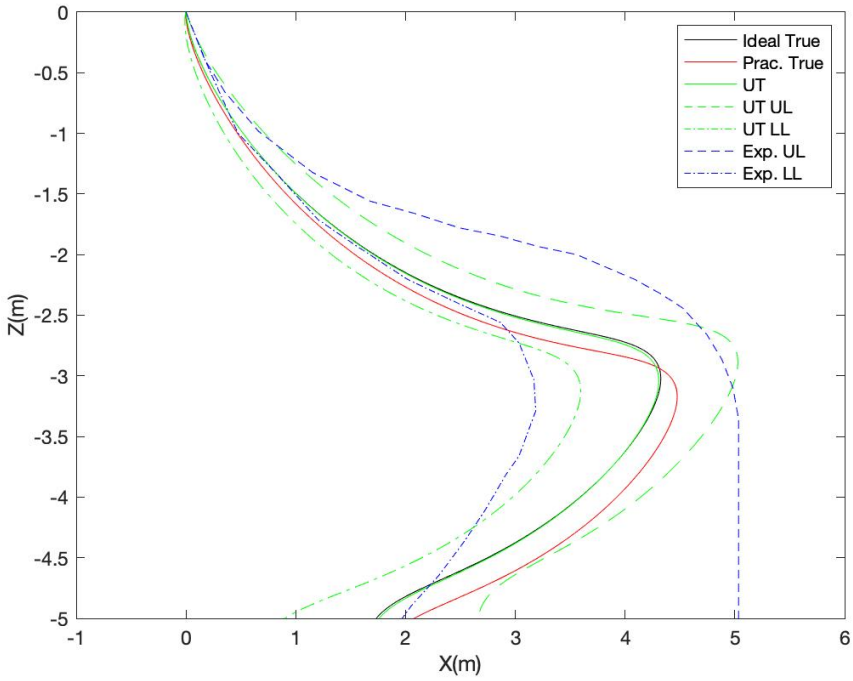

Figure 42 Trajectory prediction at the drop angle 45° using UT method (Probability=0.5)

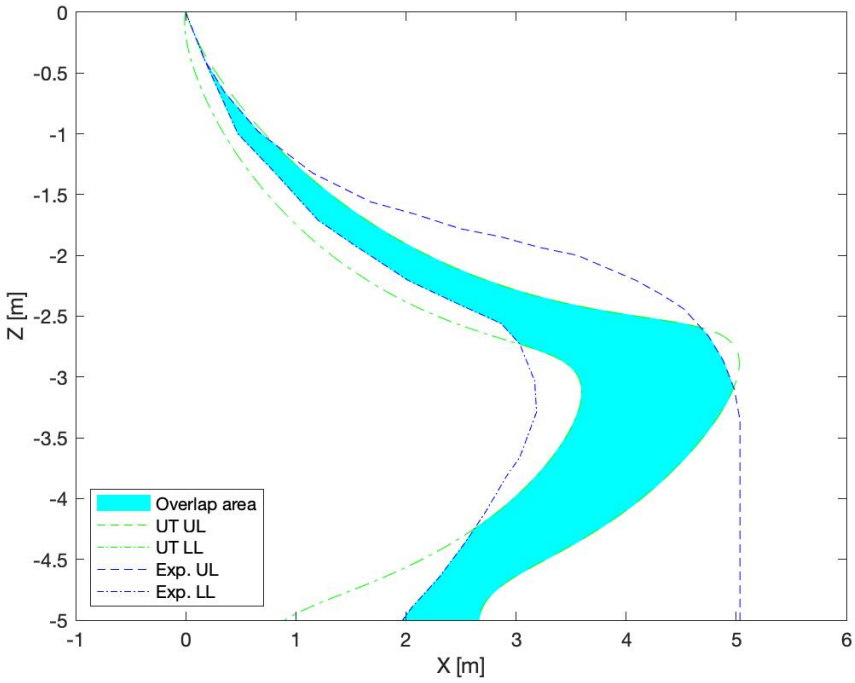

Figure 43 Overlap area between UT method and experimental envelope with the drop angle 45°(Probability=0.5)

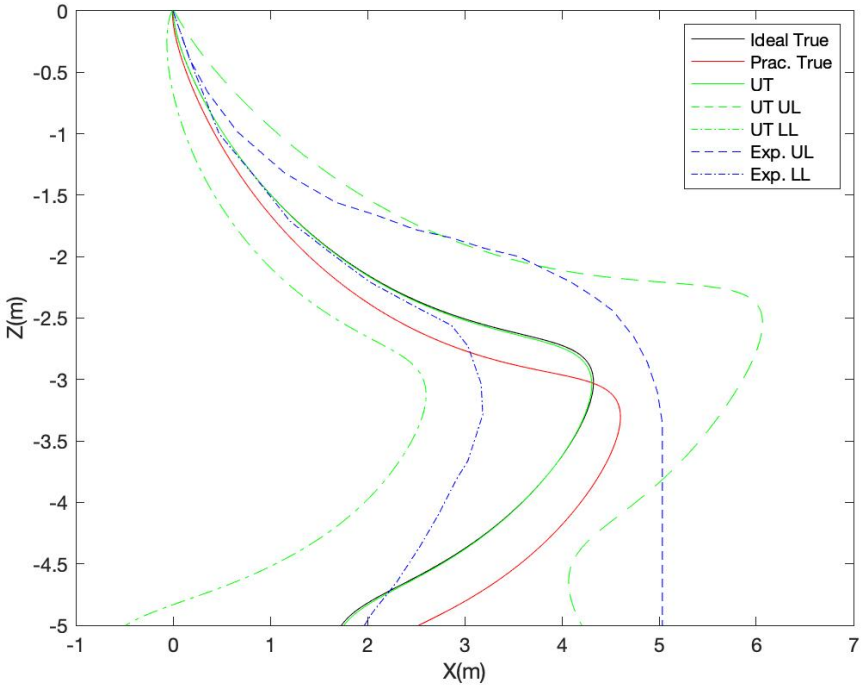

Figure 44 Trajectory prediction at the drop angle 45° using UT method (Probability=0.9)

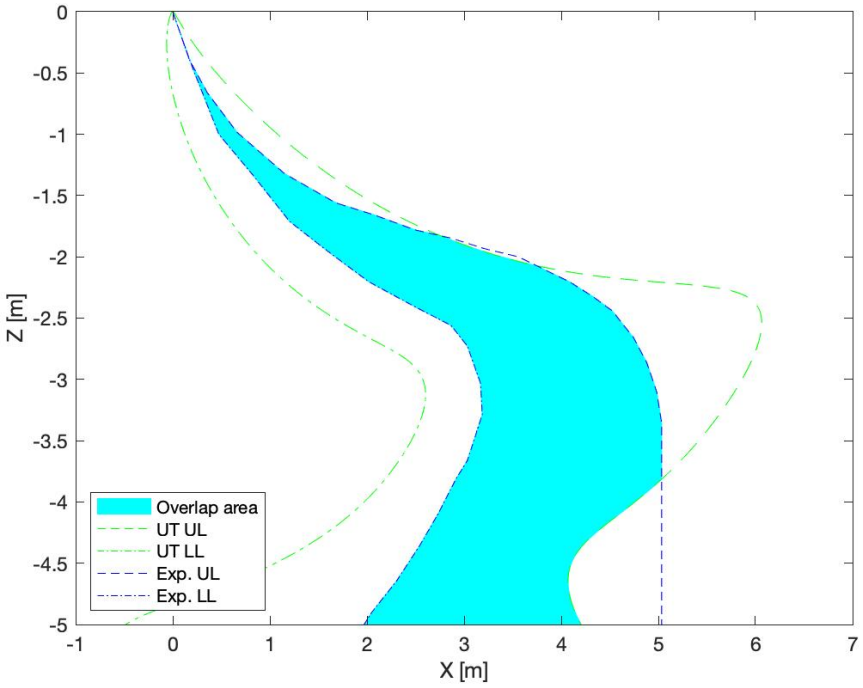

Figure 45 Overlap area between UT method and experimental envelope with the drop angle 45°(Probability=0.9)

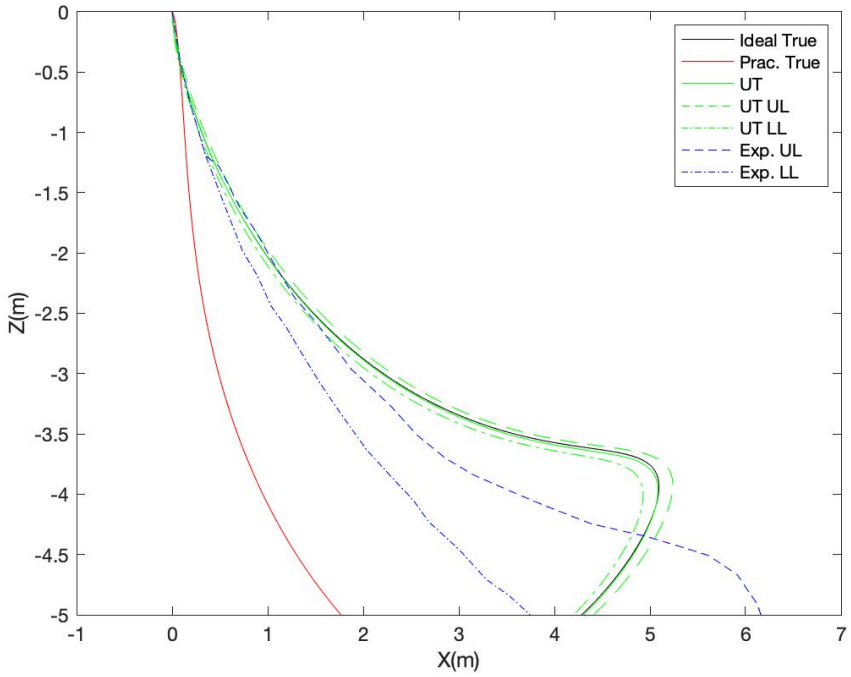

Figure 46 Trajectory prediction at the drop angle 60° using UT method (Probability=0.1)

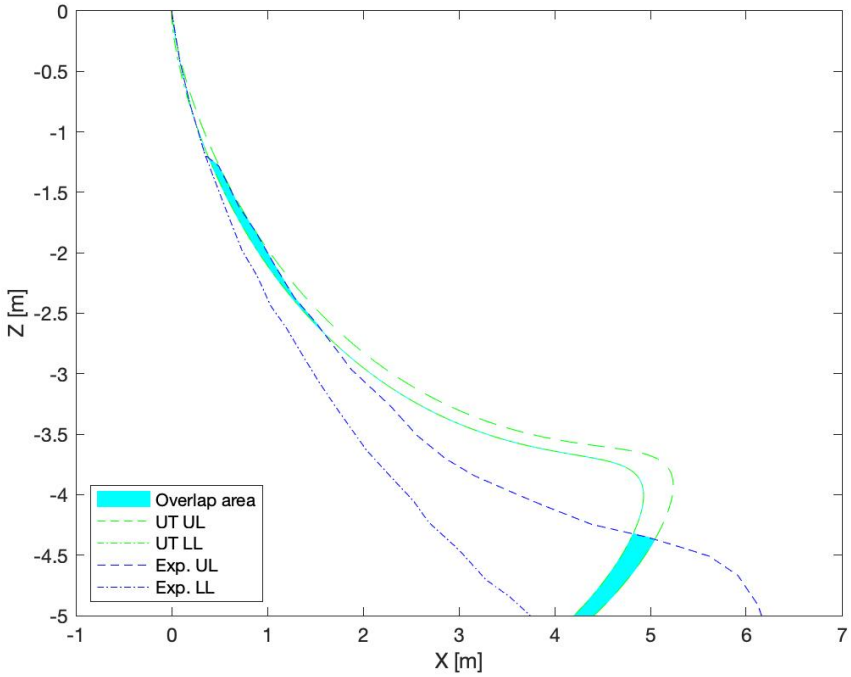

Figure 47 Overlap area between UT method and experimental envelope with the drop angle 60°(Probability=0.1)

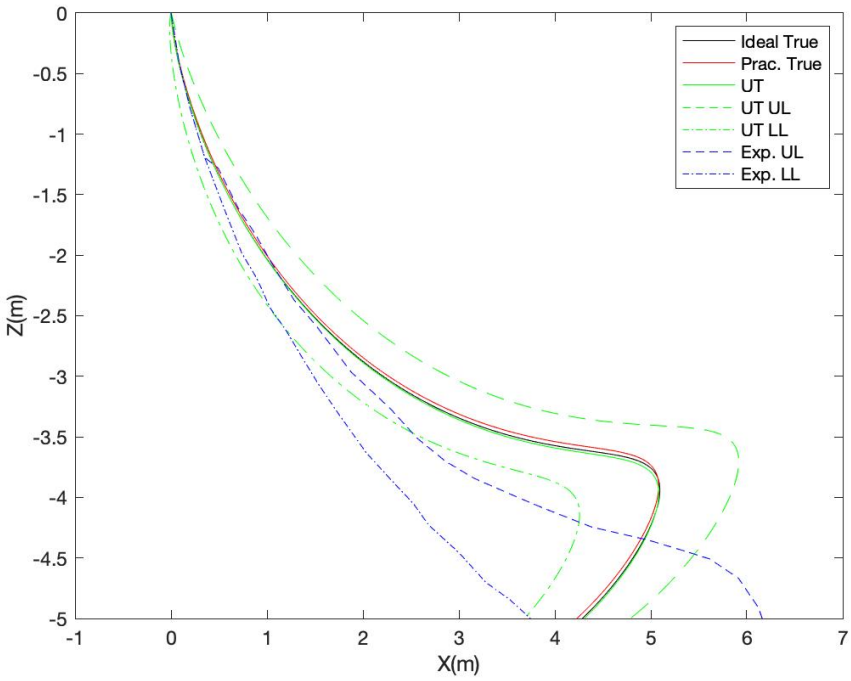

Figure 48 Trajectory prediction at the drop angle 60° using UT method (Probability=0.5)

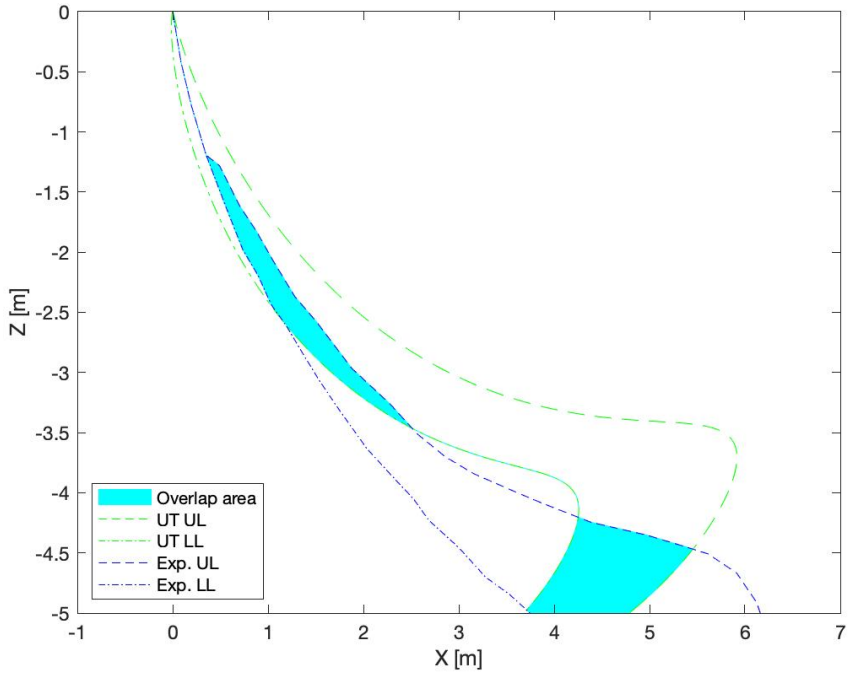

Figure 49 Overlap area between UT method and experimental envelope with the drop angle 60°(Probability=0.5)

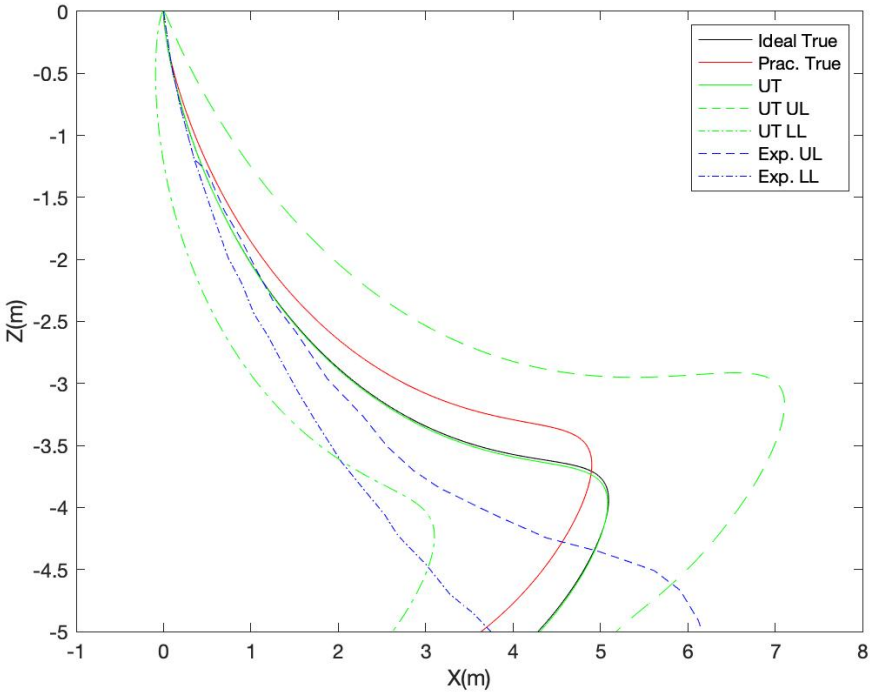

Figure 50 Trajectory prediction at the drop angle 60° using UT method (Probability=0.9)

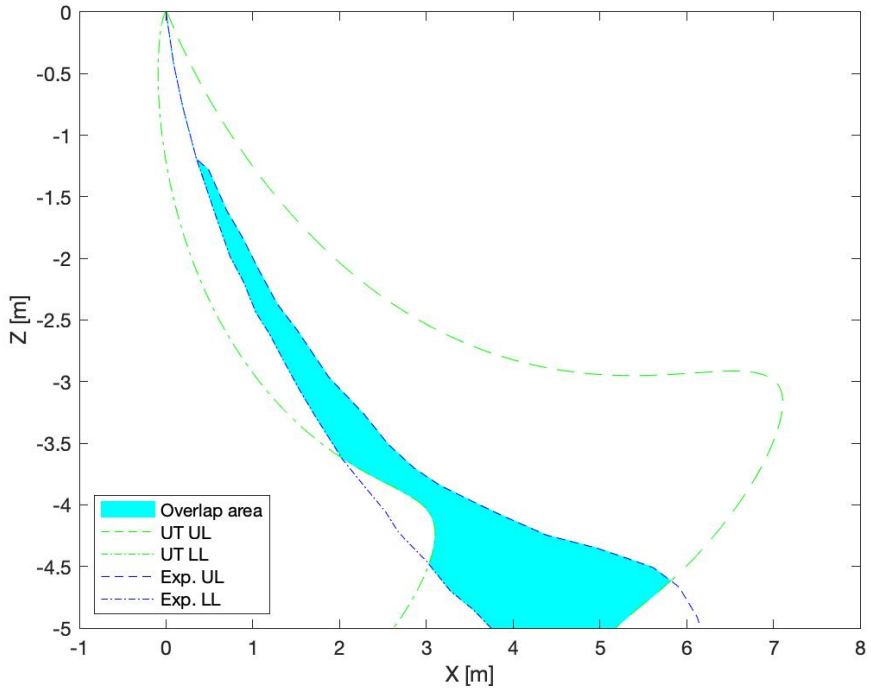

Figure 51 Overlap area between UT method and experimental envelope with the drop angle 60°(Probability=0.9)

VITA

Yi Li was born in Guangdong, China. He received the B.S. degree in Civil Engineering from Qingdao Technological University in 2015. He joined the NAME graduate program at the University of New Orleans in 2017, to pursue a Ph.D. degree in Applied Science and Engineering.